THE IMPORTANCE OF ELECTRIC MOTOR THERMAL MANAGEMENT AND THE ROLE OF POLYMER COMPOSITES IN AXIAL COOLING

The Importance of Electric Motor Thermal Management and the Role of Polymer Composites in Axial Cooling

By
Cody Rhebergen

A thesis submitted in partial fulfillment of the
requirement of the degree of

Master of Applied Science

Presented to the Faculty of the

Department of Mechanical Engineering

At

McMaster University

Hamilton, Ontario

McMaster University MASTER OF APPLIED SCIENCE (2015) Hamilton, Ontario

(Mechanical Engineering)

TITLE: The Importance of Electric Motor Thermal Management and the Role of Polymer Composites in Axial Cooling

AUTHOR: Cody Rhebergen, B.Eng (McMaster University)

SUPERVISOR: Dr. Ali Emadi

NUMBER OF PAGES: 101

Lay Abstract

The desire to increase the power density of electric machines is becoming an increasingly popular challenge, especially in the automotive industry. With the advent of electrified powertrains as an alternative solution to conventional internal combustion powered vehicles, the topic of increasing electric motor performance is becoming very attractive area of research. An important aspect of electric motor performance is the way in which the generated thermal energy is managed. Through material development and innovative motor design, there exists the opportunity to cool electric motors through cooling paths flowing axially through the stator. This 'axial cooling' design has the opportunity to greatly increase motor cooling by removing thermal energy directly from its main source, the motor windings. The following research is aimed at the thermal design of the axial cooling and the role in which thermally conductive polymer composites play in order to enhance motor cooling.

Abstract

The following research investigates the effect that axial cooling channels will have on the performance of the thermal management system of a hypothetical switched reluctance motor. A baseline motor with no axial cooling will be compared to an identical motor with the innovative cooling design implemented. This will allow for a direct comparison of the two designs, with a quantifiable performance increase determined through thermal simulations.

The ability of a polymer composite to transfer heat to the axial cooling channel is also explored. A detailed material selection process is discussed with the result being an epoxy polymer composite. The material development of a thermally enhanced polymer composite is then investigated to achieve a maximum thermal conductivity material that can exist within the stator slot to achieve enhanced thermal energy transfer.

Dedication

I dedicate this thesis to my parents, Pete and Evelyn Rhebergen. There is no one else who I could ask for to be so encouraging and loving as I worked through the past two years. I would like to thank my Mom for being the love and support that she provided as I finished this work. I would also like to thank my Dad for teaching the meaning of hard work and to persevere even when things were tough. The work ethic that you instilled in me is the only reason I was able to achieve what I have. Your teachings will always be with me, even when you no longer are.

Acknowledgements

I would like to thank my supervisors Dr. Emadi for providing me with the opportunity to pursue my graduate studies in hybrid vehicle technology.

This research was undertaken, in part, thanks to funding from the Canada Excellence Research Chairs (CERC) Program.

I would also like to thank Liz Rowan and Jason Lo at CanmetMATERIALS for their support in the aspect of materials and polymer science.

My gratitude also goes out to my peers on the McMaster Formula Hybrid Team and McMaster Engineering EcoCAR3 team, the past years with you are truly remarkable and unforgettable.

Table of Contents

Table of Figures

Index of Tables

Abbreviations

BEV	Battery Electric Vehicle
HEV	Hybrid Electric Vehicle
PHEV	Plug-in Hybrid Electric Vehicle
FCV	Fuel Cell Vehicle
SRM	Switched Reluctance Motor
MMF	Magnetomotive Force
LFA	Laser Flash Analysis
DSC	Differential Scanning Calorimetry
AlN	Aluminum Nitride
HBN	Hexagonal Boron Nitride

1. Introduction

Electrified Powertrains for Automotive Applications

The automotive industry is in the process of adopting electrified powertrain technologies in an effort to reduce the total amount of emissions produced. Electrified powertrains offer a more energy efficient solution to vehicle propulsion when compared to conventional internal combustion powertrains. Electrified powertrains are able to drastically reduce the energy consumed in a given drive cycle when a typical internal combustion engine has an efficiency of less than 30%, whereas electric motors used in Battery Electric Vehicle (BEV) can achieve an efficiencies upwards of 90% [1]. By adopting and electrified powertrain in some way, either through a full BEV topology or a hybrid electric architecture, auto manufacturers are beginning to reduce the vehicle emission of their fleets as a whole.

Although vehicle electrification has the capacity for increased efficiency in vehicle transportation, there are also some drawbacks. Things such as vehicle range, charge time and vehicle cost are all contributing factors to the challenge of vehicle electrification. One of the major drawbacks to the electrified vehicle revolution is the increased cost of implementing an electrified powertrain complete with energy storage and motor control units. One of many examples of this increased cost of electrified powertrain is the 2015 Honda Accord and the 2015 Accord Hybrid. The base Accord starts at a price of $25,863 whereas the Accord Hybrid starts at $31,518. A study was completed on the incremental costs associated with the

implementation of various electrified powertrain [2]. Included in the research presented are the cost of vehicle technologies such as turbo and diesel engine's, Hybrid Electric Vehicles (HEV), various degrees of Plug-in Hybrid Electric Vehicles (PHEV), Fuel Cell Vehicles (FCV) and Battery Electric Vehicles (BEV). Since different degrees of vehicle electrification are possible, three PHEV vehicles are analyzed that are capable varying amounts of electric-only vehicle range. PHEV-10, PHEV-30 and PHEV-60 denote plug in hybrid electric vehicles that are capable of 10, 30 and 60 miles of electric only range.

Table 1 Incremental Cost Associated with Various Electrified Powertrains [2]

Component	Turbo	Diesel	HEV	PHEV - 10	PHEV - 30	PHEV - 60	FCV	BEV
Drivetrain								
Motor/Controller	N/A	N/A	$600	$800	$800	$800	$1400	$1400
Engine/Transmission	$500	$700	$200	$100	$100	$100	$3500	-$3500
Fuel Cell	N/A	N/A	N/A	N/A	N/A	N/A	$3000	N/A
Energy Storage								
Battery	N/A	N/A	$900	$1500	$2800	$4600	$1000	$12000
H_2 Storage (150L)	N/A	N/A	N/A	N/A	N/A	N/A	$1800	N/A
Miscellaneous								
Exhaust	$0	$500	$0	$0	$0	$0	-$300	-$300
Wiring, etc.	N/A	N/A	$200	$200	$200	$200	$200	$200
Charger	N/A	N/A	N/A	$400	$400	$400	N/A	$400
Total	$500	$1200	$1900	$3000	$4300	$6100	$3600	$10200

Table 1 shows that any sort of powertrain electrification results in an increased vehicle cost compared to a conventional internal combustion powertrain. Of these electrified powertrains, the more electric focused the vehicle is, the greater the cost of the vehicle. This increased cost is due to several components required in electrified vehicles such as energy storage, power electronics and electric motors. A

considerable contribution to the increased cost in electrified powertrains is the use of expensive electric traction motors. A major component of the cost of electric machines can be attributed to the use of rare earth permanent magnets, which many motors utilize for automotive applications. Permanent magnet electric machines are often utilized in electrified vehicles due to their high power density and relatively small packaging. In order for the cost of traction motors used in the automotive industry to decrease, it is necessary to move away from their reliance on permanent magnets. Permanent magnet free motors such as Switched Reluctance Motors (SRM) are attractive solutions for low cost motors that can be used for traction.

SRM's are attractive electric machines for use in automotive applications due to their high and variable speed, low manufacturing cost and relatively simple and robust design. SRM's have numerous advantages over other types of electric motors including lower manufacturing cost. Since SRM's do not require permanent magnets for their operation, their cost to manufacture is has potential to be lower than a motor that utilizes permanent magnets. Other advantages of an SRM include fault tolerant operation and robust construction. Given these characteristics specific to an SRM, this type of motor becomes an attractive solution to automotive applications [3], [4].

One of the most important factors in electric motor design is the ability for the motor to dissipate the thermal energy that is generated through inefficiencies. By developing novel methods of removing thermal energy from electric motors, the overall power output of an electric machine can be increased. In the case of

permanent magnet-free motors, the majority of the thermal energy generated through the operation is by way of the losses associated with the copper windings. Since the thermal efficiency of copper is dependent on the temperature of the copper, it makes the motor windings a very attractive area of improvement in terms of motor cooling. By effectively cooling the copper windings of an electric machine, there is the potential to increase the overall efficiency of the motor. Additionally, by maintaining a high degree of cooling, the power output of the motor can be increased. It can therefore be proposed that effectively cooling the motor's copper windings is very important to the increase of the power density of electric machines [5].

The following research will focus on the aspect of cooling of high power electric machines and describe in details the effect of axial cooling channel within a motor stator. Additionally, the role of polymer composite materials and how they affect the thermal management of a hypothetical electric motor are explored. Topics such as current methods of heat extraction and heat sources in a motor will be discussed in Chapter 2. In Chapter 3, current models for the prediction of particle filled polymer composites will be investigated. Chapter 4 details the production of a thermally conductive polymer composite for use within the motor stator as a means of heat removal. The issues that arise due to implementation and the results of thermal conductivity testing are also included. Chapter 5 outlines the finite element model that was created to simulate the heat transfer within the motor. Boundary conditions, mesh quality and assumptions are all discussed in detail. Additionally,

chapter 5 will include the results and discussion of the produced thermal simulations. Both axial and non-axial cooled motors are analyzed and compared to determine the effectiveness of axial cooling channels on the peak motor temperatures. Finally, chapter 6 will investigate the sensitivity of the model to changes in various input parameters.

The Concept of Axial Cooling

Since the motor cooling is of critical importance in the area of electric motor design, it is beneficial to develop advanced technologies that are capable of more effectively removing thermal energy. The following sections justify the need to research novel cooling solutions in electric motors. The concept of axial cooling is proposed and compared to a conventional jacket cooling system. Additionally, a detailed material analysis is completed to determine the starting point for the axial cooling design.

Justification for Axial Cooling

The majority of electric motors available today use the conventional jacket cooling method in order to remove thermal energy from within the motor. In this process, thermal energy is removed from the circumference of the motor by way of a cooling fluid that flows through passages running through the motors casing. This cooling process requires heat generated from critical components, such as motor windings, to conduct through the stator, into the motor casing and then into the cooling fluid to be evacuated. Since there is such a large distance to travel and many interfaces to conduct through, there is a high thermal resistance preventing the generated

thermal energy from being removed. Figure 1 Displays three different paths that exist for heat to conduct to a point of heat extraction, which are the blue areas of the diagram. It a realistic case there are almost infinite paths in which heat could conduct, however this simplified process assumes three of the highest resistance paths that can be taken. This assumption will allow for a simple comparison between a baseline motor cooling design and a cooling design with additional axial cooling channels implemented.

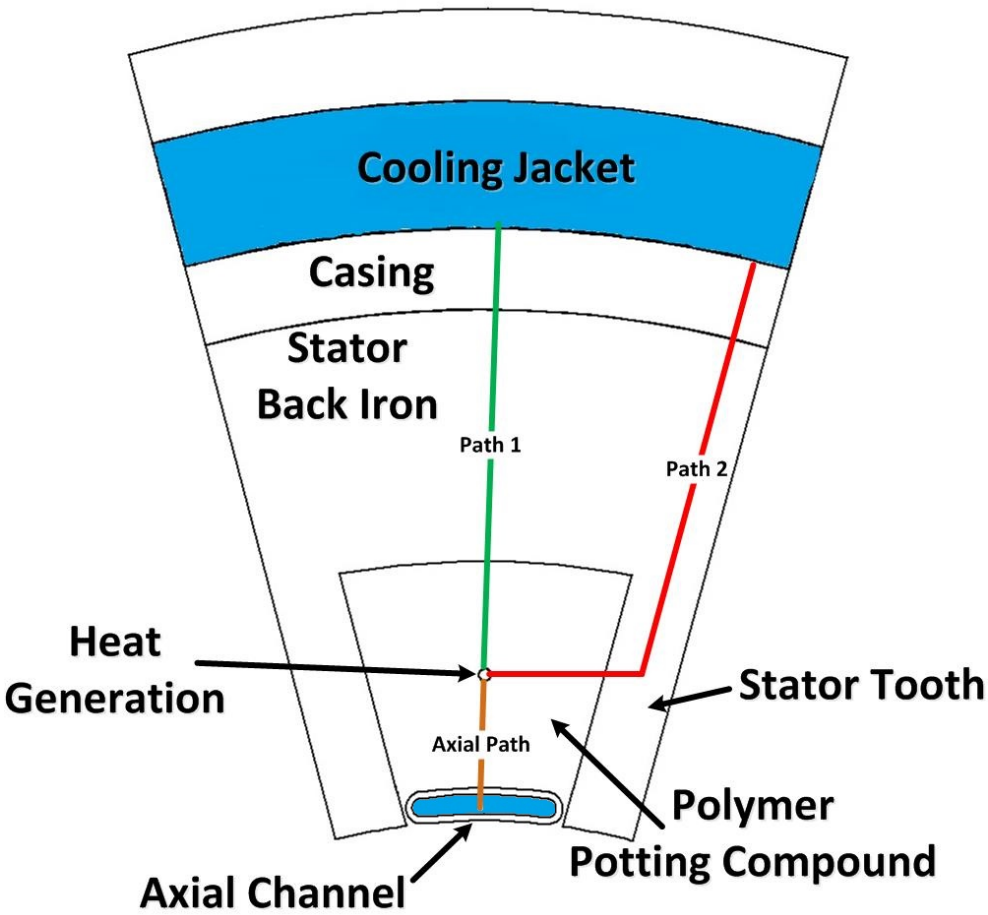

Figure 1 Conduction Paths From Highest Resistance Coil

Thermal energy is assumed to be generated from a single point source that is a copper wire located at the center of the stator slot. This wire has a 0.1mm polymer insulation surrounding it, which is a conservative estimate for wires used in motor windings. The stator slot is assumed to be surrounded in a polymer-potting compound that attaches wire to the stator and axial cooling channel.

Figure 2 displays an equivalent thermal circuit that the heat from the motor coil experiences as it conducts to the jacket cooling fluid.

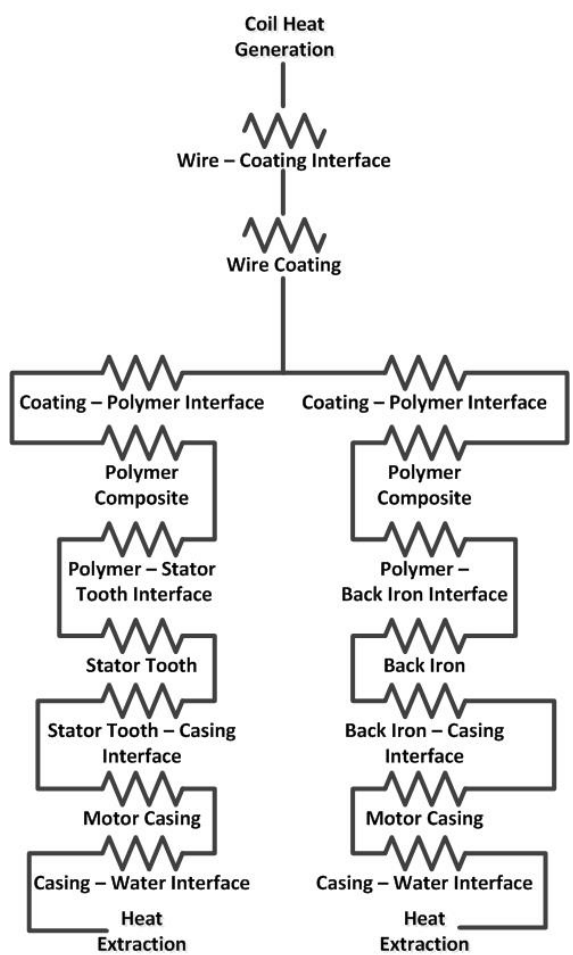

Figure 2 Thermal Circuit of a Baseline Jacket-Cooled Motor

Heat conduction in a baseline jacket cooled motor conducts from the point of heat generation though the polymer potting compound and into the stator at both the tooth and the back iron. The following simple lumped parameter study assumes that these conduction paths work in parallel with one another. The thermal resistance network pictured in Figure 2 includes all thermal resistances caused by interfacing materials. Of these interfaces resistances, the only one to have a considerable effect on the overall thermal resistance is the interface between the stator and the motor casing. All other interface thermal resistances are assumed to be negligible and are not considered. Figure 3 displays the simplified thermal resistance of the baseline cooled motor design.

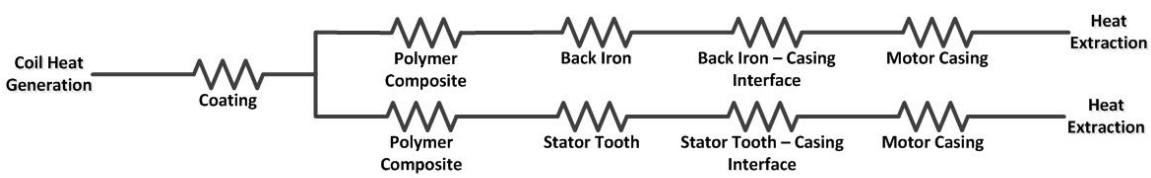

Figure 3 Simplified Thermal Network for Baseline Motor

A simple lumped parameter analysis can be completed to determine overall thermal resistance experienced by the coil present in the center of the stator slot. Thermal resistance of the individual components in the thermal network can be calculated by the following equation:

$$R = \frac{l}{\kappa A} \quad (1)$$

The thermal resistance, R, is calculated using the length of the conduction path, l, the thermal conductivity of the medium, κ, and the cross sectional area of the conduction path, A.

Using a given motor stator design, the cross sectional area and length of the conduction paths can be investigated. Figure 4 shows the length of the conduction paths for both a jacket cooled motor. The length of the conduction paths of the axial cooled motor design are also pictured, this cooling design will be discussed in the following section.

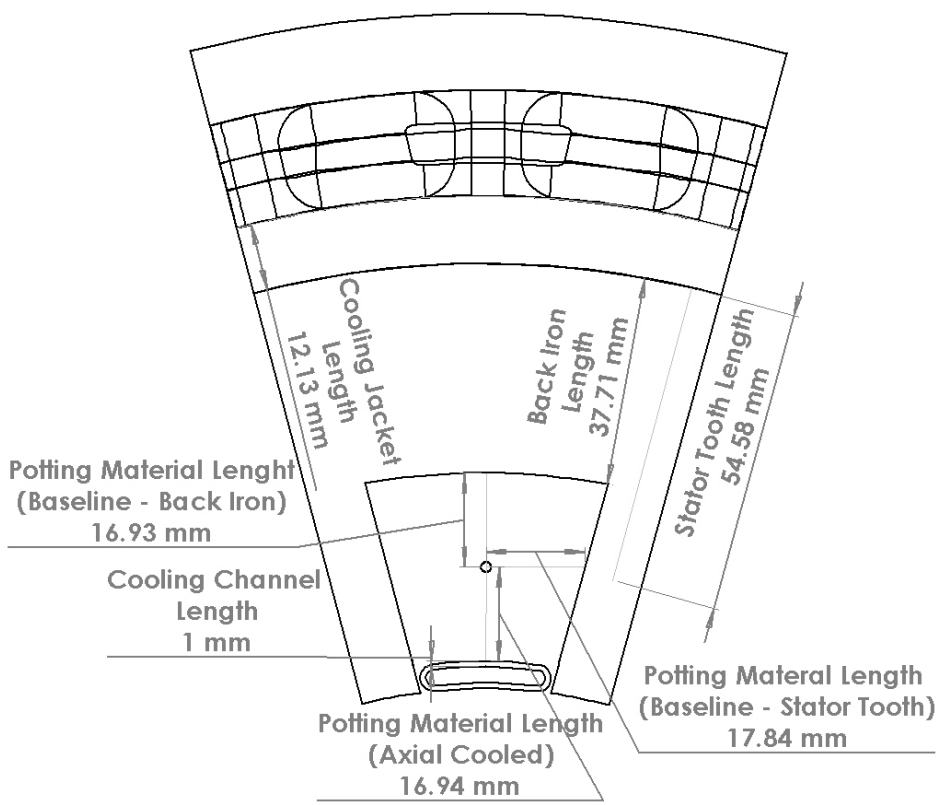

Figure 4 Lengths of Conduction Paths

To determine the equivalent thermal resistance of conduction Path 1 and Path 2, the components of the respective paths were added in series.

$$R_{Series} = R_n + R_{n+1} + R_{n+2} \quad (2)$$

Once the total thermal resistance of the two conducting networks was determined, the total thermal resistance of both Path 1 and Path 2 could be calculated by adding their values in parallel. Parallel addition of the resistances of Path 1 and Path 2 was computed using the following equation:

$$\frac{1}{R_{Parallel}} = \frac{1}{R_{Path\ 1}} + \frac{1}{R_{Path\ 2}} \quad (3)$$

Table 2 displays the values of the calculated thermal resistances for the jacket cooled baseline motor.

Table 2 Thermal Resistance Calculation of Jacket Cooled Baseline Motor

	L (mm)	A (mm^2)	Thermal Conductivity (W/mK)	Material	Resistance (m^2K/W)
Conduction Path 1					
Coil Coating	0.10	361.10	0.20	Polymer	1.38
Potting Material	17.84	3794	2	Conductive Polymer	2.35
Stator Tooth	54.58	2461.00	43.00	Steel	0.52
Motor Casing	12.13	2461.00	205.00	Aluminum	0.02
				Path 1 Total	4.25
Conduction Path 2					
Coil Coating	0.10	361.10	0.20	Polymer	1.38
Potting Material	16.93	2524	2	Conductive Polymer	3.35
Stator Back Iron	37.71	3660.00	43.00	Steel	0.24
Motor Casing	12.13	3660.00	205.00	Aluminum	0.02
				Path 2 Total	4.99
				Baseline Total	2.30

In the jacket-cooled motor, the major resistances were found to be the thermal conduction through the wire coating and through the polymer-potting compound. The most logical way to increase the efficiency of thermal energy removal is to reduce the thermal resistance experienced by the energy generated from the copper wire. This can be done through a number of ways, reduction in the conduction length, an increase in the conduction area or increasing the thermal conductivity of the medium in which heat passes. Given constraints within the motor, such as stator tooth length, stator back iron thickness and stator material, improvements in thermal resistance experienced by a cooling jacket design is somewhat constrained.

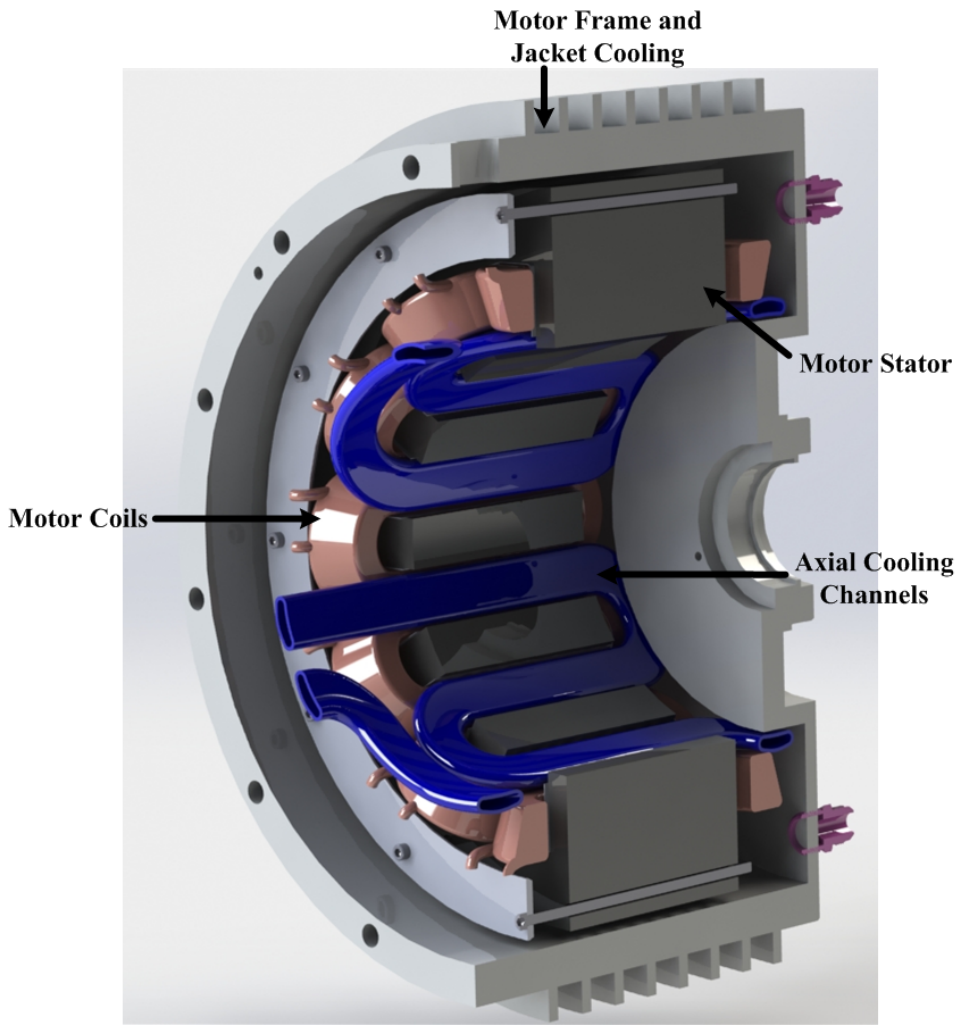

Figure 5 Axially Cooled Stator Cross-Section Schematic

When considering the overall thermal resistance from the copper wire, it is advantageous to investigate the critical thermal resistance, which is the copper wire's polymer coating and polymer potting compound. Since the wire's coating is a constrained area of the design, the only area of improvement is then the polymer-potting compound. The simplest way to achieve a reduction in thermal resistance is to reduce the length of the thermal network from the coils to the point of heat

extraction. Therefore, it is desirable to locate a point of heat extraction as close as possible to the coil itself.

By packaging a cooling channel to flow axially between the stator teeth of the motor, the length in which thermal energy needs to travel before extraction is reduced. Figure 5 shows a cross-sectional view of a motor that has axial cooling channels flowing through the stator slot. By packaging cooling channels within the stator slot, an extra conduction network is created in parallel to the thermal conduction network of a traditional jacket cooled motor.

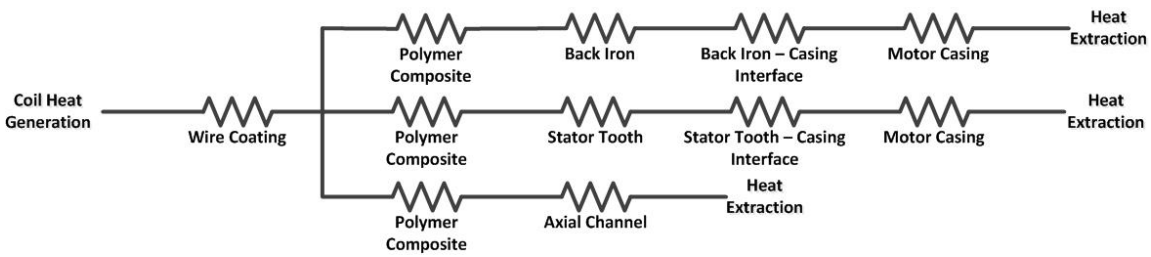

Figure 6 Thermal Circuit of an Axial Cooled Motor

In the axial cooling thermal circuit, the major sources of thermal resistance are still same as in the baseline jacket-cooled design. However, by adding these conductive networks in parallel, the overall thermal resistance of the cooling system is reduced, and more heat can be removed from the copper wire.

As in the lumped parameter analysis for the jacket-cooled motor, the resistances of the axial cooled motor can be determined in a similar method. Once the thermal resistance of the axial conduction path is determined, the total thermal resistance of a motor with axial cooling implemented can be determined.

Table 3 Thermal Resistance Calculations

	L (mm)	A (mm^2)	Thermal Conductivity (W/mK)	Material	Resistance (m^2K/W)
Coil Coating	0.10	361.10	0.20	Polymer	1.38
Potting Material	16.90	3054.40	2.00	Conductive Polymer	2.77
Axial Cooling Channel	1.00	2473.65	20.00	Conductive Thermoplastic	0.02
			Axial Cooled Total		4.17
			Combined Total		1.48

For the baseline jacket cooled motor, thermal resistance from the coils to the outer cooling jacket is 2.3 m^2 K/W while the resistance of the axial cooling channels is 4.17 m^2 K/W. By adding the total resistances of each thermal network together in parallel, the combined thermal resistance experienced by the coils to the cooling medium is 1.48 m^2 K/W.

By completing this relatively simple lumped parameter thermal analysis, it is clear that the addition of axial cooling channel has the potential to have a significant benefit to the motor in terms of thermal energy removal. Even with a relatively high thermal resistance to the axial cooling channel, the fact that there are two cooling networks working in parallel, helps to significantly reduce the overall thermal resistance experienced by the motor coils.

With axial cooling implemented, not only is more heat evacuated, it is also being removed from the hottest and most critical components of the motor, the coils. Since the motor coils rely on a polymer coating to prevent a short circuit occurring in the motor, they are typically the thermal limiting factor with H-class wire only being

able to withstand 180^0C. By enhancing coil cooling, the motor will be able to achieve lower coil temperatures for equal amounts of coil current density. Therefore, higher motor output power can be achieved through enhances in coil cooling, provided that the motor is electromagnetically designed for the higher output power. An additional benefit to maintaining low coil temperatures is the ability for increased coil conductive efficiency. Copper has a temperature coefficient of $0.00397K^{-1}$, meaning that as the temperature of copper increases, its electrical resistivity increases. At 180^0C, the maximum operating limit of H-class wire, the electrical resistivity of the copper resistivity is 160% greater than copper at 25^0C [6]. Therefore, it is beneficial to maintain lower coil temperature by cooling the windings directly, which will increase the operating efficiency of the coils [5].

Material Selection Analysis

Now that it is known that axial cooling has a significant effect on the overall thermal resistance of the motor, it is now required to define the material properties required for the components that are to be added into the stator slot. The following analysis determines materials that have the potential of existing within the stator slot to achieve axial cooling in an electric motor.

When incorporating materials into the stator slot of an electric motor, there exists a possibility of reducing motor efficiency due to the reduction of magnetic flux passing between the stator and rotor. Since switched reluctance motors depend on an electromagnetic flux between the motor and stator to transmit torque to the rotor,

any interference in this linkage would result in deceased motor efficiency. Given that the goal of axial cooling is to increase the motor's overall efficiency, any alteration to the flux path between the rotor and stator goes against what the design is trying to achieve. With implementation of axial cooling, it is important to utilize materials that will not be affected by the electromagnetic flux or to affect the motor's electromagnetic flux path. That is, the material existing in the stator flux must be immune to generating losses when exposed to a changing electromagnetic flux, and must not act as a conduction path for flux to flow. A way of quantifying this material attribute is through the magnetic reluctance of the material, which is analogous to electrical resistance in an electrical circuit [7]. Reluctance is defined through the following equation:

$$\mathcal{R} = \frac{l}{\mu_0 \mu_r A} \quad (4)$$

Where $\mathcal{R}$ is magnetic reluctance, l is the length of the flux path, μ_0 is the permeability of free space, μ_r is the relative permeability of the material and A is the cross-sectional area of the flux path.

Magnetic reluctance of the material existing within the stator slot is of great concern because if a material with a high relative permeability is introduced into the stator slot, there is potential for the motor's flux linkage to decrease. This occurs due to the lower resistance for magnetic flux to flow through the stator slot rather than through its intended path, through the rotor. By only considering slot materials that have a low relative permeability, it is possible to maintain the intended flux path

between the stator and rotor without any additional losses [8]. Additionally, electrically conductive materials existing within the stator slot may have an adverse effect on the motor efficiency. If an isotropic metallic material were to exist in the stator slot, any stray magnetic flux that passes through it could generate induced currents and heat, similar to eddy current losses that occur in the steel portions of an electric motor. For this reason, it is beneficial to implement an electrically insulating material to form a thermal conduction network from the coils to the axial cooling channel.

In addition to the electrical and magnetic properties of the slot material, there are also thermal properties that the slot material must be able to achieve. The material that is to be implemented in to the stator slot must also have a high thermal conductivity. Since the purpose of the slot material is to conduct heat away from the motor coils, it is beneficial to have a high thermal conductivity. Finally, the slot material must be able to withstand the maximum temperatures of H-class motors, which is 180°C

Using Cambridge Engineering Software (CES), a detailed material selection analysis could be completed to determine a material that has the desired metrics described above. A plot was created that compared the thermal conductivity (y-axis) to the maximum operating temperature of a number of different materials.

Using the filtering tools in CES, electrically conductive materials and highly permeable materials were eliminated from consideration. The materials eliminated from this filtering are the grey regions shown in Figure 7. Since there were too many

materials to name, they were grouped into regions of the type of material. The only materials left for consideration after the filtering were polymers such as epoxies, phenolics, and some thermoplastics like Polyetheretherketone (PEEK). These materials are very good in the desired areas of electrical conductivity and permeability as polymers are electrically insulating and have a low relative permeability. However, polymers are very poor in thermal conductivity, which is what the main goal of the stator slot material is in an axial cooling.

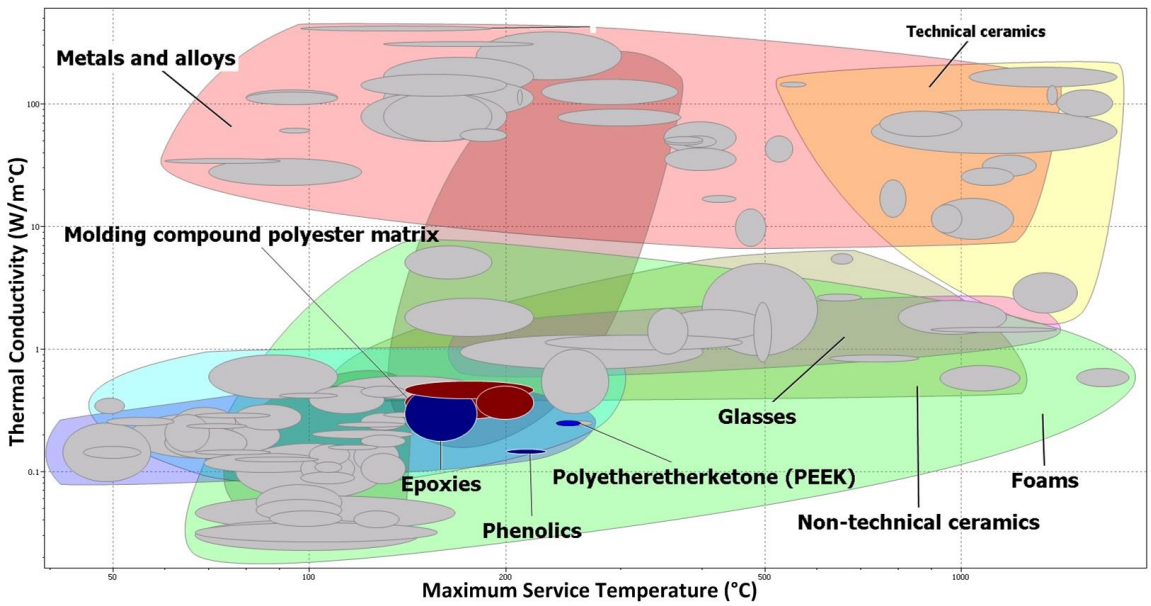

Figure 7 Stator Slot Material Selection

To increase the thermal properties of polymers, it is possible to mix a thermally conductive filler material into the epoxy to develop a thermally conductive polymer composite.

Mixing in conductive powders such as graphite, aluminum nitride (AlN) or boron nitride (HBN) can increase the thermal properties of a polymer. These thermally conductive powders can exist within the polymer matrix to form a conductive

thermal network to extract thermal energy from the motor coils and conduct it to the axial cooling channel [9]. Ceramic filler materials, such as boron nitride and aluminum nitride, exhibit electrical insulating properties while maintaining high thermal conductivity. These material attributes make them a very attractive choice for a polymer composite filler material. Graphite is also a very conductive material, both electrically and thermally. To avoid any possible issues caused by having an electrically conductive material in the stator slot, using graphite as filler material was not considered.

Table 4 Polymer and Filler Material Data [10], [11], [12], [13]

Material	Thermal Conductivity (W/mK)	Density g/cm3	Relative Permeability	Particle Size (μm)
Hexagonal Boron Nitride	30 (∟) -600(∥)	2.1	>5	5
Aluminum Nitride	170	3.31	>10	5

HBN is an anisotropic material with a hexagonal crystal structure; therefore it has two different values for thermal conductivity. The first value in the thermal conductivity that is perpendicular to the hexagonal crystal structure. The second value is the thermal conductivity that is parallel to the crystal structure. The effect of this will be discussed in the thermal testing section.

There is some debate on the intrinsic thermal conductivity of HBN with some reports having values as high as 600W/mK and other reporting only 120W/mK in the in plane direction [14], [15], [16]. Therefore, there is a large uncertainty in the

intrinsic thermal conductivity of HBN. Further thermal testing will determine the effectiveness of HBN increasing the thermal conductivity of the polymer.

Other consideration on filler material such as size and shape of particle are also very important factors for enhancing the thermal conductivity of polymers. The effect of these filler attributes on the polymer composite the will be discussed in the polymer development chapter of the following work. Additionally, the design decisions on filler size and shape and how the effect the design at a system lever will also be explored.

Objective of Research and Project Scope

The following research will quantify the benefit of axial cooling in a generic switched reluctance motor through the use of FEA simulation. A thermal management design of an axial cooling system will be created based off of a given design of a hypothetical switched reluctance motor. The stator and coil dimensions of the motor were constrained, and thus axial channel packaging is also constrained. Furthermore, the electromagnetic design of the motor is considered out of the scope of this project and is not discussed.

The development of a thermally conductive polymer composite is explored. This material development is necessary to provide a thermal conduction path from the motor coils to the axial cooling channel. In doing this, the performance of the axial cooling design can be increased as the design has an increased ability to transport thermal energy to the point of heat extraction. Although there is a considerable

amount of research completed in the area of conductive polymer composites, there exists an additional design challenge of implementation when considering polymers for use axial cooling. A further objective of the following research is to develop a polymer that can be implemented into a motor stator, while still maintaining its high thermal conductivity.

Finally, thermal modeling through finite element analysis will quantify motor peak temperatures and temperature gradients. A theoretical increase in power output of the motor can be suggested due to the increased cooling from the axial cooling channels. Since the following thermal design assumes a constrained motor and coil design, the feasibility of the magnetic design required to achieve the suggested theoretical maximum power output is not considered.

A baseline motor that uses a jacket-cooled design will be compared to a design that utilizes axial cooling channels to cool the motor coils. By directly comparing the two designs using identical simulation boundary conditions, it will be possible to determine the performance increase associated with the implementation of axial cooling channels. The final objective of this project is to develop an axial cooling system that can be implemented into any motor stator, provided that the space within the stator is allocated in the preliminary motor design to package the cooling channels.

2. Review of Motor Losses and Current Cooling Technologies

Motor Loss Contributions

With the growing popularity of hybrid-electric and pure electric automobiles, the issue of thermal management in electric machines becomes extremely important. One very critical issue with electrical motors is the generation of heat. Without sufficient thermal management, high temperatures can prematurely degrade temperature-sensitive motor components such as insulations, magnets, or bearings.

The challenge of thermal management is even more prevalent in power dense machines as a high power density also results in a high thermal generation density. With these electric motors, an effective thermal management system is difficult to implement, as packaging becomes increasingly challenging. Through rigorous thermal analysis and prototype testing, it is possible to develop new thermal management systems that have the ability to improve electric machine performance, even with a reduced packaging size. Small power dense motors are attractive for use in automotive applications as they reduce packaging difficulties within the vehicle and have the ability to reduce the overall weight of the vehicle. With the implementation of axial cooling, motors can be created that have increased power density and thus can improve overall weight and packaging of future vehicles.

Electric machine losses can be broken down into two groups: mechanical loss and electromagnetic loss. Mechanical losses primarily consist of bearing friction, and windage losses, windage losses being the aerodynamic losses associated with a

rotating salient rotor. Mechanical losses are generally small compared to electromagnetic losses and are beyond the scope of this research due to the fact that they are typically generated at a significant distance away from where the axial cooling channels are to be packaged. Major electromagnetic losses that are considered as significant sources of thermal energy are copper losses, hysteresis losses and eddy current losses, which are discussed in more detail below.

Copper Losses

Electric machines utilize magnetic fields to produce torque, thus requiring a current carrying conductor surrounding a ferromagnetic material. In an electric motor, torque is created through the creation of magnetic flux paths. The strengths of these magnetic fields are determined, in part, by the magnetomotive force (MMF) applied. The MMF generated in a motor stator is defined as the product of the number of turns in the winding and the current running though the winding.

$$\mathrm{MM}F = Ni \quad (5)$$

Since the MMF is in some way related to the amount of torque produced in an electric motor, it is beneficial to have a high MMF. To achieve this, either the number of turns in the coils need to increase, or the current running though the coils. Therefore, it is beneficial to have a high amount of current passing through the copper in the motor windings. However, a high current density in the motor windings results in a high amount of losses [17].

Since copper is typically the material of choice for motor windings, we refer to these losses as copper losses. Copper losses found within the motor windings are determined as the square of the current multiplied by the sum of the wires electrical resistance plus any associated conductor eddy current losses. Conductor eddy current losses are a function of excitation frequency, machine geometry and the design of the coil [17].

$$P_{loss} = I^2(R_{DC} + R_{AC}) + P_{eddy} \quad (6)$$

Even though a high current density is desired from to create a large MMF, the losses associated with current through the copper windings are exponential. That is, at high current values, a small increase in current results in a very large amount of generated heat.

As mentioned in the introduction of this work, copper's ability to conduct electricity is dependent on the temperature of the copper. As the temperature of the coil increases, the resistance of the copper can increase as much as 160% at 180°C when compared to room temperature. This means that the losses generated through the copper coils increases as temperature increases, which in turn generates more thermal energy. It is the objective of the motor's thermal management system to remove the heat from the windings as quickly as possible as to not increase its temperature beyond the wire insulation operational limit.

Eddy losses of the copper coils are generated by alternative magnetic flux passing through the conductor. The magnetic flux that cause these losses occur from 2 main

sources, from current passing through a nearby conduction (proximity effect), or from leakage flux from the motor stator.

The proximity effect is caused by the flow of alternating current from an adjacent conductor. Since a conductor with a current passing through it generates its own magnetic field, as per the right hand rule, this magnetic field can influence adjacent conductors. The alternating magnetic field from an adjacent conductor induces a small, circular current into its neighbor as it passes through. A way of imagining these types of loss is by picturing an oar passing through water while rowing a boat. As the oar passes though the water, small areas of turbulence generate circular vortices in the water. These vortices are analogous to the eddy current generated when magnetic flux is passed through a conductor. The induced currents experience an electrical resistance on their own, and thus, generate heat [18].

These types of losses are not only due to magnetic fields created by adjacent conductors, but also from flux produced by the stator. The copper windings create a magnetic flux in the stator tooth to be used to create torque in the rotor. Although this flux is concentrated in a certain direction, some flux leaks from its intended path and passes through the coils. Flux leakage is usually produced in a high density near the tip of the stator tooth. Therefore, any copper coils that are in closer proximity to the stator tooth tip are prone to a greater amount of losses [19], [20].

Core Losses

Other than the heat generated by the copper losses in the windings, losses in the iron core of electrical machines is also of significant importance. Core losses are perhaps one of the biggest areas of uncertainty when estimating the thermal energy generated in electric motors. Core losses are mainly dependent on excitation frequency, flux density and loss characteristics of the electrical steel, but also depend on less quantifiable factors such as lamination manufacturing method and internal stresses due to manufacturing. The two loss mechanisms that are of concern within the motors core are eddy current and hysteresis losses.

All core losses are generated in either the rotor or stator of a magnet free electric motor. In permanent magnet motors, additional losses are also generated within the permanent magnets themselves. The components are made of steel, which is a ferromagnetic material. A ferromagnetic material is defined as a material that has a strong positive reaction to an applied magnetic field. That means that when a magnetic field is applied to the material, the magnetic field is multiplied, resulting in a stronger magnetic flux density than was originally applied. This happens through the alignment of magnetic domains within the material. Magnetic domains are small areas within the material that have their own permanent magnetism. Though an applied magnetizing force, magnetic domains align into a uniform direction. In doing this, the magnetic field in the material is increased [21], [22].

Eddy currents are the result of an alternating magnetic field being passed through a ferromagnetic material, which results in an unwanted induced current. These losses

are very similar to eddy losses generated within the coils of the motor. These induced current are minimized using electrical steel that is laminated with non-conductive sheets [7].

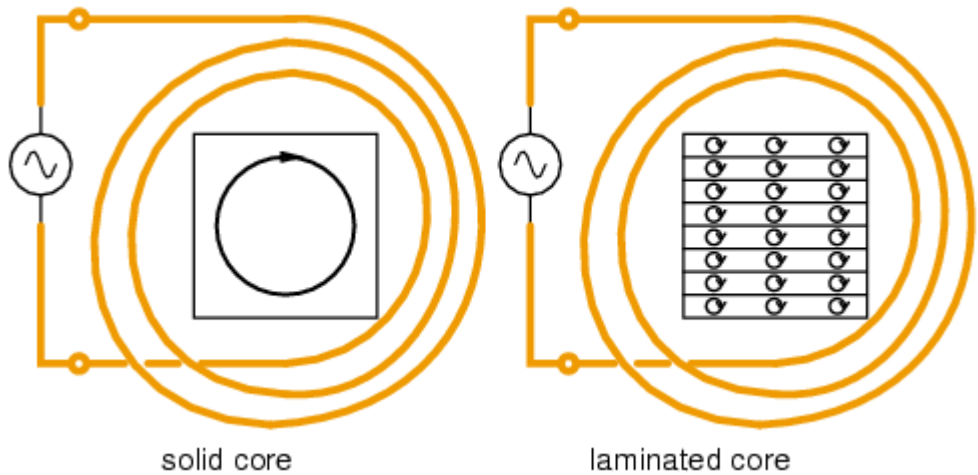

Figure 8 Reductions in Core Losses through Use of Laminated Steel [23]

Figure 8 displays the change in magnitude of eddy current losses when laminated steel is used for motor components such as the stator and rotor. It can be seen that in laminated steel, the eddy currents are constrained through insulating lamination material. This reduces the magnitude of the circular eddy current, which reduces the overall losses generated. Typically, the thinner the electrical steel laminations, the lower these losses are [24].

Hysteresis losses can be described as a resistance to the change in direction of a magnetic field within a ferromagnetic material. When electrical steel is presented with a magnetizing force, the magnetic domains are aligned into a uniform direction. Once the applied magnetic field is removed, most of the domains randomize, however some domains remain in the same orientation as the initial applied

magnetic field. The energy required to reorientation these domains into a new direction is known as hysteresis losses [25].

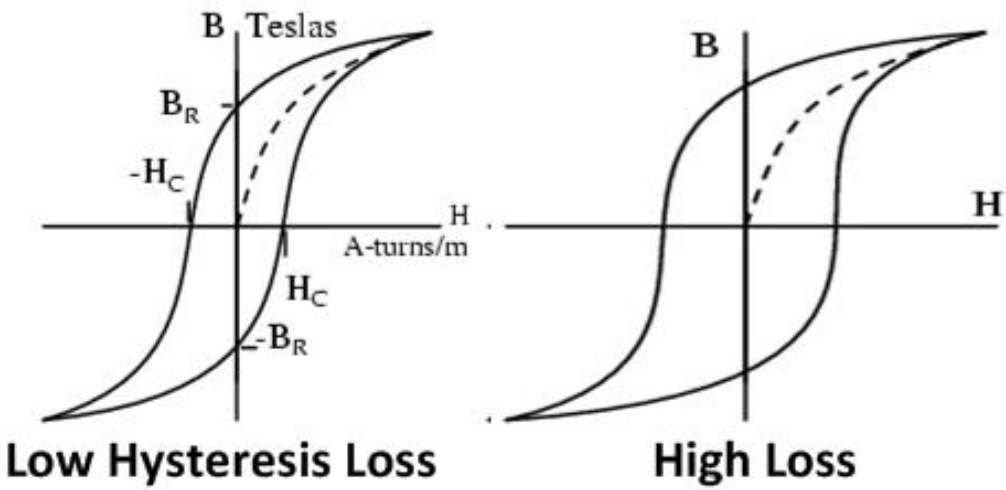

Figure 9 Descriptions of Hysteresis Losses [23]

Figure 9 demonstrates the magnetization curve, measured in flux density (B), of a ferromagnetic material given an applied magnetizing force (H). If the ferromagnetic material is not initially magnetized, as a magnetizing force is applied, the flux density within the material increases along the dotted line until it reached the point of magnetic saturation. Saturation is the point in which all domains in the ferromagnetic material are aligned into a uniform direction. If the magnetizing force is reversed, the flux density will move to point B_R, which is the point of retentivity. Ideally, with zero magnetizing force, there would be zero magnetic flux, however, not all of the magnetic domains randomize once the applied magnetic field is removed. In fact, a negative applied magnetic force is required to achieve a net zero flux density, point $-H_c$, or the point of coercivtity. It is this resistance to changes in magnetization that causes losses to occur in the stator and rotor of an electric

motor. If the hysteresis loop is wide, it takes more energy to change the directions of the magnetic domains. Thus, it is ideal for electric motors to use a ferromagnetic material that has as narrow of a hysteresis loop as possible in order to minimize losses. Eventually, magnetic saturation will be achieved in the opposite direction to what was initially applied and the same process will occur if the applied magnetic field is changed again [26]. This drastically changing magnetic field are the conditions that occur within an electric motor. Since high amount of magnetic flux are required in very short periods of time, the magnitude of magnetic flux and direction is constantly changed, resulting in a high amount of hysteresis.

Conventional Motor Cooling Solutions

Air Cooling

Air-cooling is a relatively simple form of thermal management for an electric machine when compared to a liquid cooled motor. The ability for air to pass through a motor without requiring passages or segregation from critical motor components make it a simple and cost effective method of cooling electric machines. However, air has a lower convection coefficient and heat capacity than liquids, which make it thermodynamically less effective at removing heat compared to most liquid coolants. For low power density motors this is not an issue as the amount of heat generated by losses can be easily captured with air-cooling. For more power dense motors, power is somewhat limited by the ability for air to transfer heat away from critical components such as the motor windings or the motor's steel components.

Even with considerable forced air-cooling, heat removal is limited by the heat transfer properties of air. Air cooling strategies are vast, and often vary based on the size and type of machine being cooled.

Liquid Cooling

Typically, high power density electric motors are cooled using a liquid coolant as a liquid coolant is much more effective at thermal removal when compared to air. [27] Unlike air-cooled motors, liquid cooled motors require containment methods to direct the flow of coolant.

In certain applications, it is possible that critical motor components can be completely immersed in cooling media. In these designs, the rotor and stator are mechanically isolated from each other, and the rotor is immersed in a cooling fluid. These systems are typically used for pumps and the robustness of such a system is unclear for traction applications. Any failure in winding insulations could cause instant failure if liquid coolant becomes conductive through fluid contamination or other means.

In other applications, it is not possible for critical components to be directly liquid cooled; therefore heat is required to flow through additional thermal resistances before being removed by the liquid coolant. However, liquid coolants are far superior in their heat transfer characteristics when compared to air. This allows for a greater amount of heat to be removed, although not directly from the source. This

provides some challenges, as the components that generate the greatest amount of heat, are typically the components that will fail at the lowest temperatures.

Current electric motors use many different methods to cool the motors internal components. Methods such as end turn, jacket and lamination cooling are all popular techniques used to remove heat from the motor. Some less popular designs such as axial cooling have also been researched but have yet to make their way into production of commercial electric machines.

End Winding Cooling

One area of the motor that is of considerable interest when it comes to thermal energy extraction is the motor coils, specifically, the end windings. The end windings are the section of the windings that turn around the end of the motor stator tooth. Typically, the end windings of the motor are neglected when it comes to liquid cooled motors [28]. This requires a significant amount of consideration when designing the motors thermal management system. End turn cooling is achieved by circulating a cooling fluid around the end turns of the windings. This is an effective method as the cooling fluid is in direct contact with the motor windings, because research suggests that end turns can be the hottest area inside of a motor [29] [30]. A particular design as patented by Pratt & Whitney Canada Corp, directs cooling fluid radially outward from the center of the motor to the end turn windings. The coolant is then channelled through the end turns and continues flowing radially outwards, where is captured and directed to a cooling unit. This cooling solution, as

depicted in Figure 10, provide significant winding cooling as the entire end turn is in contact with the cooling media.

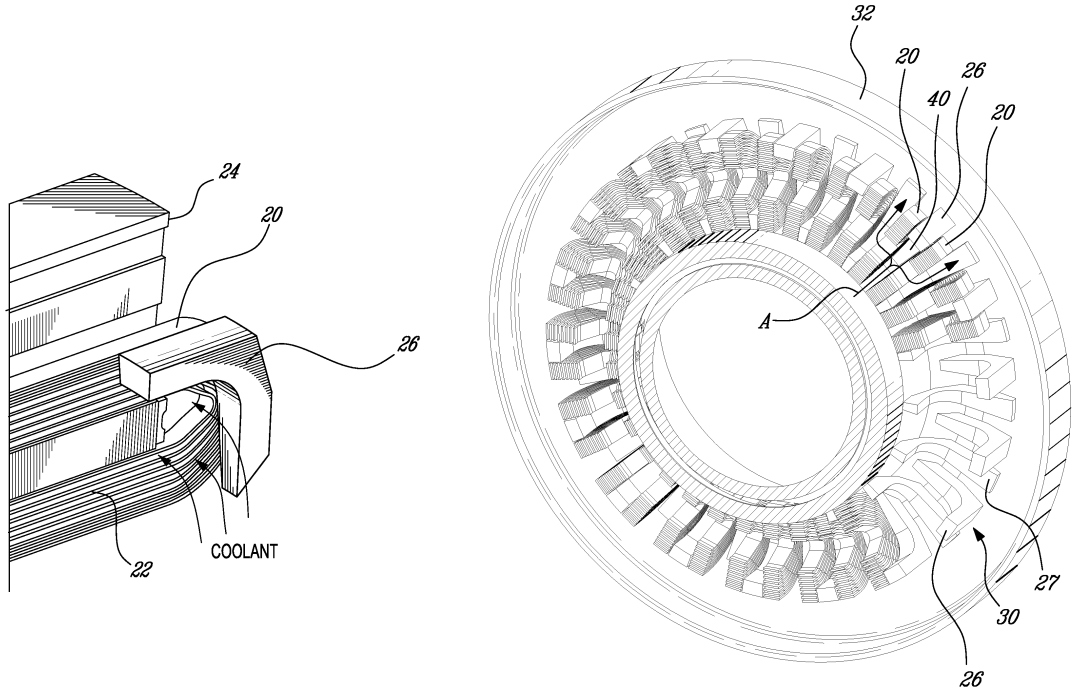

Figure 10 Winding End Turn Cooling in an Electric Machine [31]

Jacket Cooling

Cooling a motor by way of a concentric cooling jacket is the most conventional thermal management design. By flowing coolant through channels located on the outermost surface of the stator, heat is extracted radially through the motor. One issue with this design is that heat must first flow radially through the stator tooth, its surrounding components, and the motor frame itself before the liquid coolant removes the generated heat. This results in a thermal resistance that limits the

maximum rate of heat removal and thus, increases the temperature of the motors critical internal components.

A component of particular concern is the motors winding insulation. The windings are one of the motors main sources of losses, and therefore heat generation. The insulation covering these windings is very sensitive to thermal stresses. The life of the insulating is greatly reduced if this maximum operating temperature is surpassed, this would result in a short circuit in the windings and a failure in the motor [32]. For this reason it is essential for a thermal management design to remove as much heat directly from the windings as possible, as they are typically the most likely to fail first.

An existing jacket cooling design as invented by General Electric consists of pre-fabricated metal cooling tubes being cast into the motor frame.

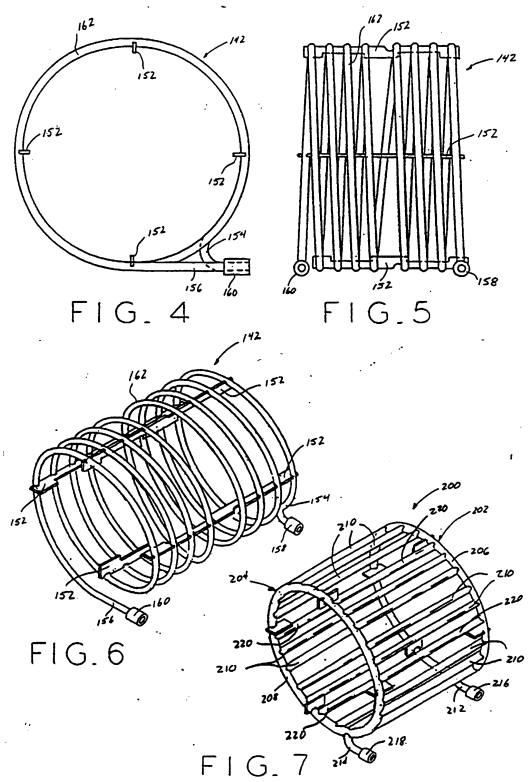

Figure 11 Pre-Fabricated Metal Cooling Channels [33]

Jacket cooling solution is very simple and easy to implement as little to no post machining of the motor frame will take place. Although this is a fairly simple design, a problem may exist with the thermal interface resistance between the bulk cast material and the cooling pre-fabricated cooling tubes.

A more advanced method for implementing a jacket cooling design is to incorporate the cooling channels directly into the motor housing [34].

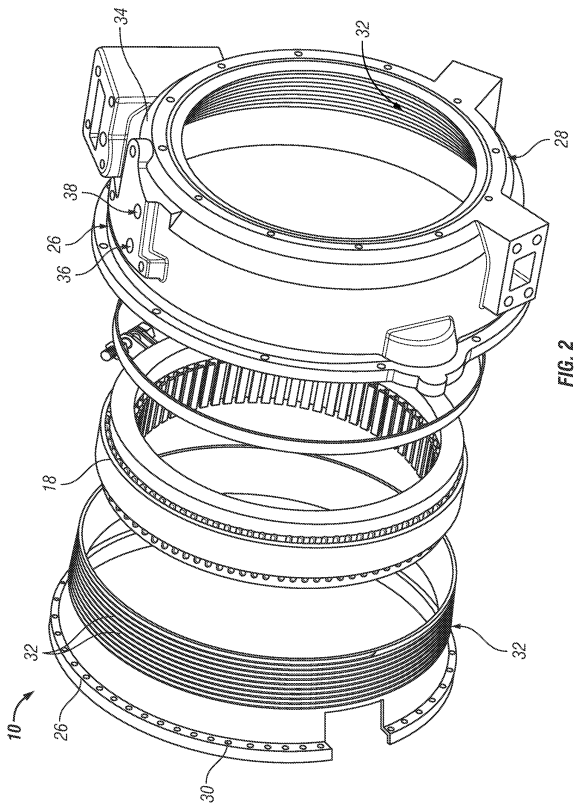

Figure 12 Integrated Cooling Channels in Motor Housing [34]

Having the cooling conduit incorporated into the motor frame itself eliminates thermal resistance created by any interface of cast aluminum onto pre-fabricated cooling tubes. This strategy provides a more efficient cooling design and potentially improved motor performance.

Passive Phase Change Cooling

This method of cooling can only be used in a sealed, non-rotating part of an electric machine. A motor stator, including the end turns, is sealed in a hermetically sealed enclosure and partially wetted with a phase changing cooling liquid. As the motor temperature increases, the cooling liquid is heated and evaporates into a vapour

state. This change in phase absorbs heat from the surface in which the liquid was heated. The vaporized coolant travels to the enclosure walls where it is cooled and condensed back into its liquid state as heat is transferred to a liquid-cooled jacket [35]. This cooling method is useful for removing thermal energy directly from motor windings, where thermal evacuation is most crucial. This is beneficial over traditional jacket cooling where heat has to travel to the jacket cooling fluid through the conduction paths described in the introduction of this work. However, a liquid phase passive phase change cooled motor requires additional design challenges, as the cooling chamber must be hermetically sealed.

Lamination Cooling

In an effort to remove heat directly from its source, designs have been produced that implement cooling channels into the steel laminations of the motor. Since both hysteresis and eddy current losses are generated in the steel laminations, it is beneficial to remove the heat generated immediately by way of a cooling fluid. In a particular design as patented by Aerovironment Inc., these cooling channels are implemented into the back iron of the stator of an electric machine. [36]

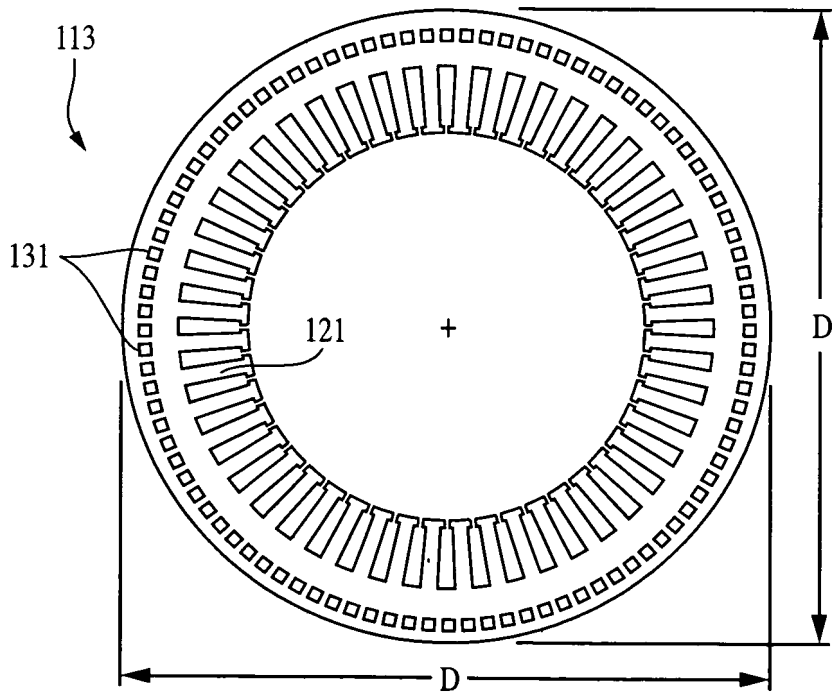

Figure 13 Back Iron Lamination Cooling [36]

Figure 13 displays the cooling channels implemented into the back iron of the stator, which directly cool the motor's steel laminations. In order to evenly divide cooling fluid among the channels, a manifold exists on both the entrance and exit of the stator to distribute and capture cooling fluid.

One drawback of this lamination cooling design is the location of the cooling channels with respect to the magnetic flux of the motor. Since the back iron of a switched reluctance motor is used as a path for magnetic flux to flow, any cavities that exist may act as a resistance to the magnetic flux path. This would obstruct the flow of magnetic flux resulting in a compromise between cooling and motor output power.

Another solution to cool the motor laminations is to create flow passages in between steel laminations. This allows large quantities of heat to be removed directly from the laminations with limited disturbance in the magnetic flux path. General Electric patented a solution to inter-laminar cooling for gas-cooled machines in 1999. Although the patent uses gas as a cooling agent, the same concepts can be applied to a liquid cooled solution.

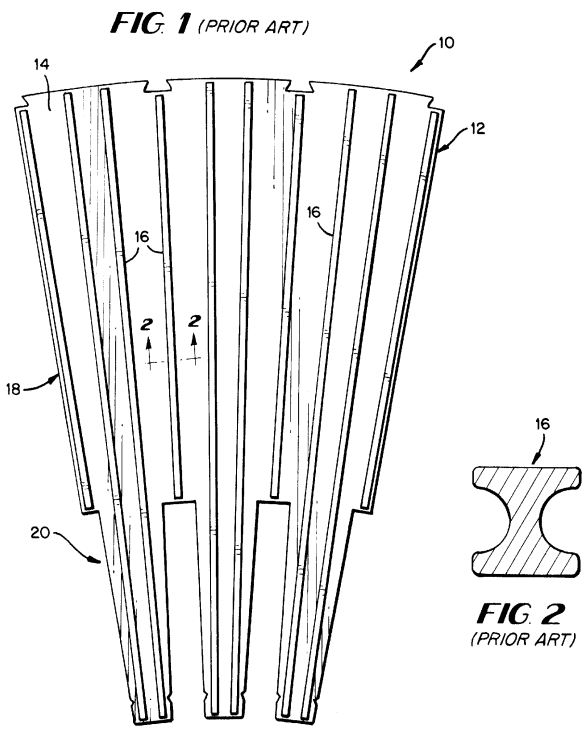

Figure 14 Stator Lamination With Radial Extending Spacer [37]

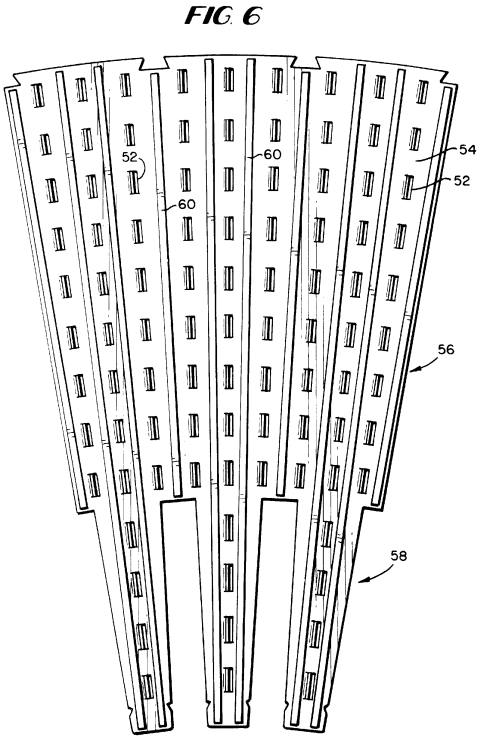

Figure 15 Radially Extending Cooling Channels with Turbulators [37]

Figure 14 shows cooling channels flowing radially along a section of the stator. Figure 15 displays a similar design to Figure 14, however flow turbulators have been added. The flow turbulators have the potential of increasing the effectiveness

of removing heat from the laminations by generating turbulent flow in the cooling media.

This design is very advantageous in terms of cooling, however, the manufacturing and assembly of the motor stator become incredibly complex. Additionally, since the amount of space between the steel laminations has increased, complex flux paths may occur.

Axial Winding Cooling

In salient machines, an opportunity to improve motor performance exists by way of axial cooling channels. Cooling channels can be implemented into the slots of the stator teeth, which would help in removing heat generated by the windings due to copper losses. This type of cooling is not popular in traction drives today as implementation of cooling channels into the stator is very difficult. Researchers, however, have implemented such systems with some degree of success [29] [38] [39].

3. Polymer Composite

Literature Review on Predictive Thermal Conductivity Models

It was discussed in the introduction that polymer materials are the most attractive solution for the encapsulation of a motor stator. Polymers are expected to exhibit no adverse effects from to presence of electromagnetic flux, and also are not expected to have an effect on the flux path within the motor. Certain polymers are able to withstand the intense thermal environment that they may experience within the motor stator. Given that polymers are typically a thermally insulating material, it is advantageous to increase the thermal properties by mixing a polymer with a thermally conductive filler material.

It is beneficial to calculate the estimated thermal conductivity of a proposed polymer composite before testing samples in order to reduce the number of trials to be completed. Estimating the thermal conductivity of a polymer, however, is much more complicated than applying the basic rule of mixtures, as one would for simple strength calculations for long fiber composites. Since complex heat transfer mechanisms occur in polymer composites, factors such as the shape, aspect ratio, volume fraction and packing factor of the filler all become very important. These factors make the dependence of filler percentage on the thermal conductivity of the bulk composite a non-linear relationship. Only by properly modeling these factors together can an accurate estimation of the thermal conductivity of a polymer composite can be made.

Several models are available for the estimation of thermal conductivity in a polymer composite, the simplest of which is the rule of mixtures. The rule of mixtures combines the thermal properties of the matrix and filler linearly based on their respective volume fractions and thermal conductivities as seen in the relationship below.

$$\kappa_c = \kappa_p \phi_p + \kappa_f \phi_f \quad (7)$$

Where κ represents the thermal conductivity and ϕ is the volume fraction. The subscripts p, f and c stand for the composite, polymer matrix and filler respectively.

Maxwell also developed a model for predicting the thermal conductivity of polymer composites with spherical particles at low volume fractions [13].

$$\kappa_c = \kappa_f \frac{\kappa_p + 2\kappa_f + 2\phi_f(\kappa_p - \kappa_f)}{\kappa_p + 2\kappa_f - \phi_f(\kappa_p - \kappa_f)} \quad (8)$$

Bruggeman improved on Maxwell's model for dilute suspension of non-interacting spheres in a polymer matrix with the following relationship.

$$1 - \phi_f = \left(\frac{\kappa_f - \kappa_c}{\kappa_f - k_p}\right)\left(\frac{\kappa_p}{k_c}\right)^{1/3} \quad (9)$$

These relationships are accurate for predicting the thermal conductivity of polymer composites at low volume percent filler. They may not be useable for this project, as it is desired to have high thermal conductivity and therefore high concentrations of filler. [40] [41] [42]

Agari and Uno decided to build on the existing models to create and estimation that considered the series and parallel conduction paths in composites. Agari and Uno

hypothesized that conduction through polymer composites is due to the formation of conductive paths between filler particles. These conductive paths form exponentially as the filler concentration is increased. Their model was built off of the Maxwell model for non-interacting conductive spheres in polymer suspension.

$$\kappa_c = \kappa_f \frac{\kappa_p + 2\kappa_f + 2\phi_{af}(\kappa_p - \kappa_f)}{\kappa_p + 2\kappa_f - \phi_{af}(\kappa_p - \kappa_f)} + \phi_f \phi_f^{\phi_f - 2/3} C^2 \kappa_p \quad (10)$$

$$\phi_{af} = \left(1 - \phi_f^{\phi_f - 2/3}\right) * \phi_f \quad (11)$$

Where ϕ_{af} is the volume fraction of filler particles not contributing to forming conductive chains and ϕ_f is the volume fraction of filler particles contributing to the formation of conductive chains. C^2 is an experimentally determines constant which is a measure of the likeliness of random assembly of conductive chains. [41], [43]

Agari and Uno published very impressive results on the predicted thermal conductivity of polymer composites in their journal article that was published in 1985. Agari and Uno claimed that their model was accurate up to 30 volume percent filler.

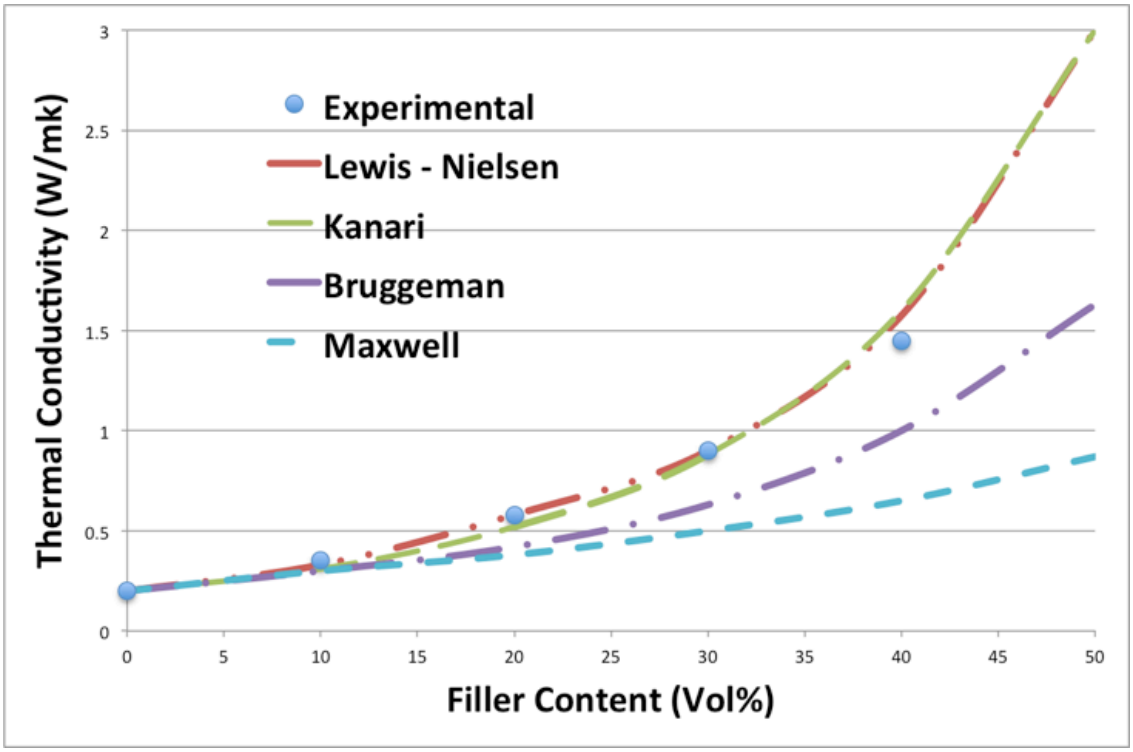

Figure 16 Comparison of Predictive Models against Experimental data [43]

Table 5 Nomenclature for Figure 16 [43]

● ● ● ● ●	Experimental data
– – – –	Kanari
- - - - -	Maxwell-Eucken curve
● - ● - ●	Bruggeman curve
- ●● - ●● -	Nielsen curve

Although the Agari and Uno models display very accurate thermal conductivity estimations for high filler concentrations, their model is not widely used huge to the complex determination of experimentally determined constants. [41]

The most widely used of all models developed to estimate the thermal conductivity of a polymer composite is the Nielsen equations. There is some debate on the accuracy of the Nielsen model at elevated filler concentrations with different

sources predicting different upper limits of the model. Some models predict that the Nielsen model can accurately predict thermal conductivity above 30 volume percent filler. [13], [44] Other sources state that the limit of the Nielsen model is below 30 volume percent filler. [45] Since different sources report different accuracies of the Nielsen model, it can be speculated that the accuracy of the predictions heavily depends on the experimental procedure and testing materials

Despite the uncertainty of the predictions of the Nielsen model, it is the preferred model for estimating the thermal properties of high filler percent composting. Composites with high filler volume fractions are of great interest due to their ability to demonstrate high thermal performance. Originally, the Nielsen equations, shown below, only considered filler materials that are spherical in shape. Modifications have been made to the Nielsen model to accommodate irregular shaped particles and their packing factors.

$$\frac{\kappa_c}{\kappa_m} = \frac{1 + AB\phi}{1 - \varphi B\phi} \quad (12)$$

$$\text{Where: } B = \frac{\kappa_f/\kappa_m - 1}{\kappa_f/\kappa_m + A} \text{ and } \varphi = 1 + \frac{(1-\phi_{max})\phi}{\phi_{max}^2} \quad (13)$$

In the above relationships, κ_c, κ_m and κ_f represent the thermal conductivities of the composite, matrix and filler respectively. ϕ represents the volume percent filler and ϕ_{max} is the maximum theoretical packing factor of the filler, which mainly depends on the geometry of the particle. Table 6 below displays some packing factors for some common filler shapes and packing orders. Variable "A" considers the geometry

of the filler, specifically the filler's aspect ratio. Common values of A for several filler geometries are compiled in Table 7 [40], [43].

Table 6 Maximum Packing Fraction of Select Fillers [40], [46]

Particle Shape	Packing Order	Maximum Packing Factor (ϕ_{max})
Spheres	Hexagonal Close	0.7405
Spheres	Face Centered Cubic	0.7405
Spheres	Body Centered Cubic	0.60
Spheres	Simple Cubic	0.524
Spheres	Random Loose	0.601
Spheres	Random Close	0.637
Irregular	Random Close	0.637
Fibers	Three Dimensional Random	0.52
Fibers	Uniaxial Hexagonal Close	0.907
Fibers	Uniaxial Simple Cubic	0.785
Fibers	Uniaxial Random	0.82

Table 7 "A" Values for Common Filler Geometries [40], [46]

Filler Geometry	Aspect Ratio	A
Cubes	1	2
Spheres	1	1.5
Random Fibers	2	1.58
Random Fibers	4	2.08
Random Fibers	6	2.8
Random Fibers	10	4.93
Random Fibers	15	8.38

Given the currently available models for predicting thermal conductivity, we expect that a value of thermal conductivity can be predicted for a polymer composite with reasonable accuracy. Throughout the literature review, it was determined that the Nielsen equations are the model of choice due to its more accurate predictions at elevated filler percentages.

4. Polymer Development and Testing

As described in the material selection section of the introduction, the design criteria for the material used to conduct heat from the motor coils to the cooling channel are quite strict. The material must be able to operate up to the temperatures of H-class insulations, 180°C, must not affect the motor electromagnetically, and must not generate any additional losses. An additional consideration that was not taken into account when choosing a material and was later found to be very problematic was the viscosity of both the base polymer and of the created polymer composites. The following section describes the specific commercial materials that were selected for use in as a thermally conductive potting compound. Of the materials that were specified in the materials selection, epoxy resins were determined to be the material of choice due to their ability to be vacuum infused into the stator.

Additionally, the ability of the polymer composite to be vacuum infused will be discussed. Vacuum infusion is the desired method of implementation as it is the most popular method of stator infiltration. Other methods of polymer infiltration such as high-pressure injection molding are possible, however due to the resources available for testing, vacuum infusion was chosen as the preferred method.

Developing an Implementable Polymer Composite

Specific Material Selection

Although there is no shortage of research being completed for thermally conductive polymer composites being used for electronic applications, the aspect of uncured

polymer composite viscosity is not an area that is extensively researched. The uncured polymer composite viscosity generates issues when it comes to the implementation of the composite into the stator.

To effectively infiltrate all aspects of the motor stator and coils, the polymer composite must be able to be vacuum infused. By vacuum infusing the uncured epoxy composite into the motor, the interface resistance between the coils and the thermally conductive polymer can be minimized. However, the issue with the vacuum infusion of the polymer composite is that as more thermally conductive filler is added to improve the thermal conductivity, the more viscous the epoxy gets. Since the thermal conductivity of the polymer composite is mainly due to the addition of conductive filler, it is beneficial to have a large amount of filler material in the composite. Therefore, there exists a maximum limit of filler material that can be implemented into the uncured epoxy, while still maintaining the ability for the uncured polymer composite to be vacuum infused into the motor's stator. It was necessary to determine this limit of polymer viscosity to be able to maximize the amount of thermal conductivity that can be achieved by the polymer, while still maintaining the ability to vacuum infuse the polymer into the motor stator. Table 8 and Table 9 display the commercially available polymers and filler materials that were considered for use as a polymer composite potting compound.

Table 8 Proposed Polymer Matrix Materials

	Elan-Cast P300S (W/mK)	MG Chemicals 832HT
Thermal Conductivity (W/mk)	0.82	0.218
Maximum Operating Temperature (°C)	180	200
Glass Transition Temperature (°C)	40	68
Coefficient of Thermal Expansion (ppm)	15	140.2
Viscosity (cP)	6000	40000

Table 9 Proposed Filler Material

Filler Material	Manufacturer	Intrinsic Thermal Conductivity (W/mK)	Particle Size (μm)	Particle Shape
Aluminum Nitride	Accumet Materials	180	5	Spherical
Hexagonal Boron Nitride	Asbury	30 (∟) -600(∥)	5	Flake
Hexagonal Boron Nitride	Momentive	30 (∟) -600(∥)	50-300	Flake

Two sizes of HBN were investigated to determine the effect of particle size on the thermal conductivity of the polymer composite. Through literature research, large particle sizes are known to have a better effect on the thermal conductivity of the polymer due to several mechanisms. If large particles are used as filler material, the amount of interfaces between polymer and filler is reduced, which helps in the transfer of heat by reducing the amount interface contacts when compared to smaller particle size. Additionally, the packing factor of the large particles is better than that of smaller particle. Which aids in the amount of thermal conductivity according to the Nielsen equations [47].

As discussed in the introduction, it is important for the polymer composite to maintain electrical insulating and to have little to no impact on the electromagnetic field of the motor. For this reason, ceramic powders such as aluminum nitride (AlN) and hexagonal boron nitride (HBN) were chosen as filler materials.

Commercially available polymer materials were selected for use at a matrix material for the polymer composite. Polymers were selected that had thermal data available for them. This was done so that estimations could be made on the thermal conductivity of the polymer composite. Without the baseline thermal data of the epoxy, it would be impossible to make predictions on the maximum possible thermal conductivity that the composite could achieve. It was soon discovered that in order for the polymer composite to remain implementable, polymers with low initial viscosities would need to be used as matrix materials due to the increase in viscosity caused by the addition of conductive filler.

Determination of Vacuum Infusion Feasibility

Originally, the ElanCast and MG Chemicals epoxies were selected for use as matrix materials. While making initial test samples, it was realized that polymer composite viscosity was drastically influenced by filler concentration. This resulted in the removal of the MG Chemicals epoxy from consideration.

To test the polymer composites ability to be vacuum infused, a series of infusion tests were completed to determine the maximum volume percent filler that is possible, while still maintaining the ability to be implemented through vacuum

infusion. Since the most difficult area of the motor to infiltrate is between the individual motor windings, this was considered the infusion tests failure criteria. If the polymer composite had the ability in encapsulate the motor windings without the presence of voids, the polymer composite was considered to be successful in vacuum infusion. If the polymer composite could not properly infiltrate the windings, the test was considered a failure.

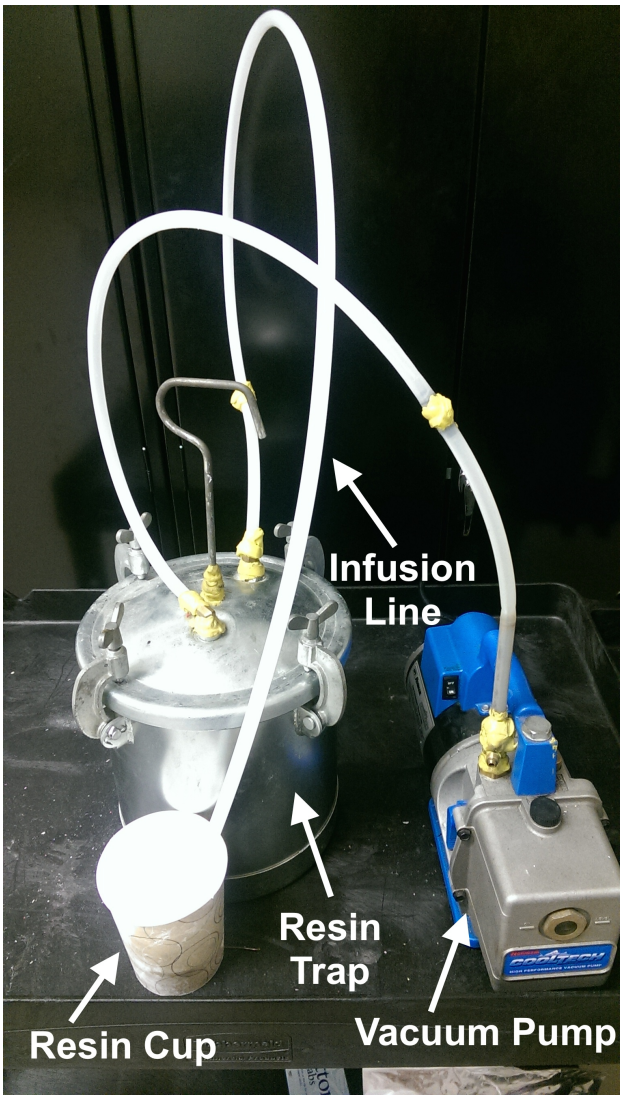

Figure 17 Vacuum Infiltration Test Setup

Figure 17 displays the test setup used to complete the vacuum infiltration testing. Uncured polymer composite was pulled by vacuum pressure from the resin cup into the infusion line. The amount of vacuum pressure used to pull the polymer composite was the maximum amount that the vacuum pump was able to achieve, about 28.5 inches of mercury. A resin trap was used in between the vacuum pump and the resin cup to catch any excess resin that might be pulled further up the infusion line than expected. This ensures that the vacuum pump is safe from being damaged by any resin being pulled into it.

To properly represent the infusion conditions of a motor stator, a bundle of coils was contained within an infusion path and infiltrated with epoxy resin. A coil-packing factor of 0.6 was used for the infiltration test, which is similar to what is achievable for wound coils for an electric motor. The length of the coils used in the infiltration test was equal to that of the motor coil length. The length of the coil was considered to ensure that completed infiltration of the entire winding could be achieved.

Table 10 Infiltration of Polymer Composites with ElanCast P300 Matrix

Filler	Filler Percentage	Infiltration of ElanCast P300
Aluminum Nitride	10	Very Good
	20	Very Good
	25	Good
	30	Not Infusible
Small Size Hexagonal Boron Nitride	10	Good
	15	Not Infusible
Large Size Hexagonal Boron Nitride	10	Not Infusible

It was learned during infusion testing that despite the benefits of large particle sizes on the thermal conductivity of the composite, the implementation of these large filler particles was very difficult. Large particle sizes were incapable of infiltrating in between he coil wires, which resulted in unsuccessful full infusion tests. At lower filler percentages where the viscosity of the uncured polymer composite was very low, the infusion tests were unsuccessful due to the large particle size not being able to fit between the densely packed coils. This caused a blockage in the infusion path and resulted in a failed infusion test. Figure 18 displays the results of infusion tests of 25 volume percent large flake HBN into Elan-Cast epoxy. It is clear to see the unsuccessful test of trying to infuse the large flake HBN.

Figure 18 Infusion Test of 25 Volume Percent Large HBN in ElanCast P300

The AlN filler material that was chosen for investigation has a much smaller particle size than the large flake HBN. This allows the AlN powder to easily fit in between the coils and results in a very good infusion test.

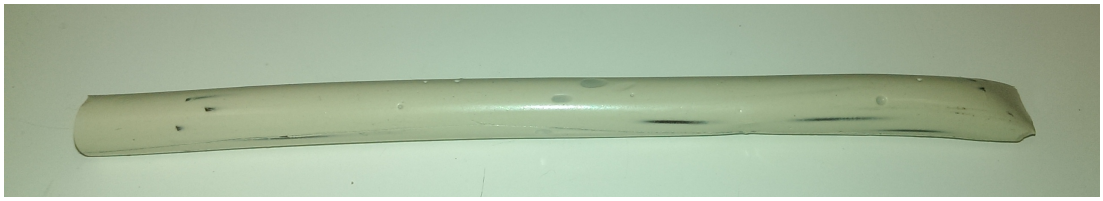

Figure 19 Infusion of 25 Volume Percent AlN in ElacCast P300

Figure 19 Displays the successful infusion of 25 volume percent AlN in ElanCast epoxy. This filler percentage was the upper limit of what was possible to be vacuum infused. After 25 volume percent, the viscosity of the uncured polymer composite was too high to achieve vacuum infiltration.

Since it is not possible to implement large flake HBN into the motor coils, it was no longer considered for use as a filler material. Instead, small flake HBN was explored as a filler material. Given than AlN and small flake HBN have similar particle sizes, about 5μm, the infiltration properties when mixed with the ElanCast Epoxy were similar. However, due to the shape of the particle on the microscopic level, the addition of the small HBN flakes resulted in very high-uncured viscosities at low filler percentages. The maximum amount of filler that could be mixed with ElanCast epoxy before vacuum infusion became unfeasible was only 10 volume percent.

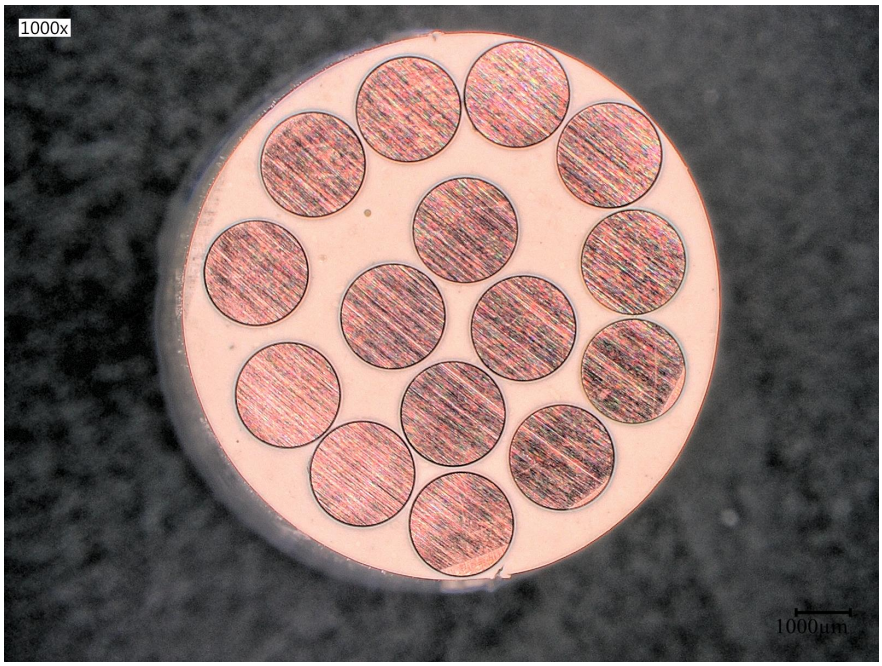

Figure 20 25 Volume Percent AlN in ElanCast P300

Figure 20 displays the cross section of a successfully vacuum infiltrated polymer composite. It can be seen that complete wetting of the coils is achieved, which results in a very low interfacial contact resistance. The infiltration is representative of both 25 volume percent AlN and 10-volume percent small flake HBN.

Polymer Sample Preparation

To test the thermal conductivity of the developed polymer composites, both laser flash and Differential Scanning Calorimetry (DSC) samples need to be manufactured. This was completed by casting of uncured epoxy composites into aluminum molds. Samples could be created, however a large amount of porosity was initially present in cured testing samples. Figure 21 displays the presence of voids in a high filler percentage epoxy composite. Since air acts as an insulator, having porosity present in the samples will have a negative impact on the overall thermal conductivity of the composite.

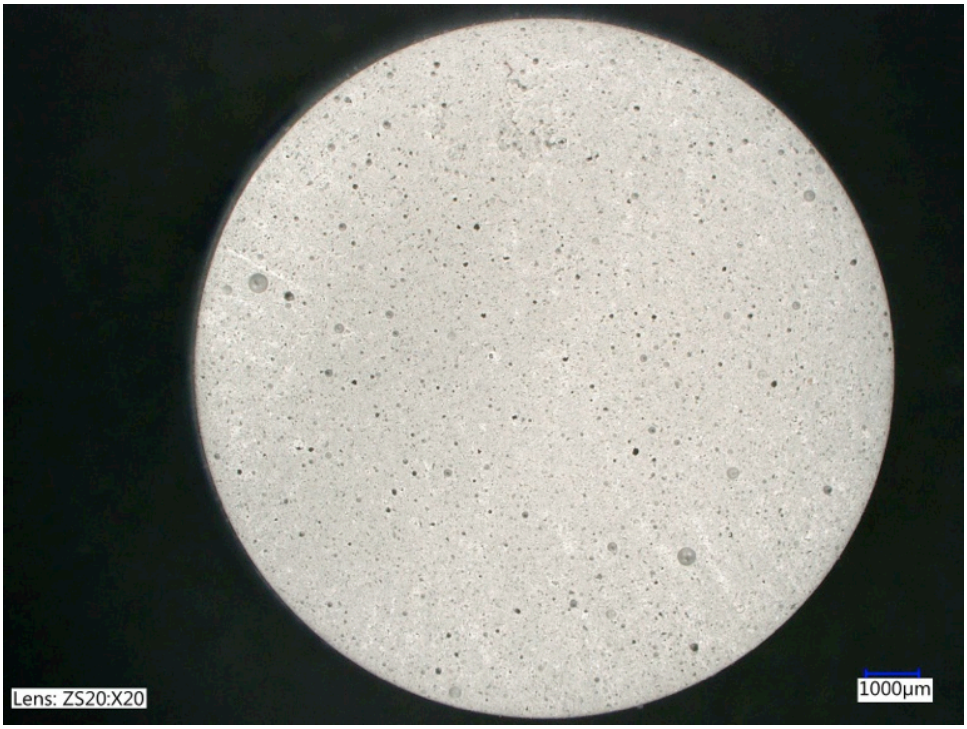

Figure 21 Presences of Voids in 40 Volume Percent Polymer Composite

These pores could be removed though vacuum degassing of the uncured polymer material. Once the resin and hardener were mixed together, the filler material could then be added. Once this was completed, the uncured composite material was placed in a vacuum-degassing chamber for 10 minutes to remove any unwanted porosity. The result of the vacuum degassing procedure can be seen in Figure 22. Since the uncured material was exposed to vacuum pressure, the majority of the porosity was removed. Once the uncured epoxy was degassed, it could be cast into the sample molds to produce test samples for thermal analysis. By comparing the microscope images of the vacuum degassed and non-vacuum degassed samples, it is evident porosity is drastically reduced by the process. It can be estimated that the

vacuum degassed sample will exhibit a higher thermal conductivity due to the preservation of thermal conduction networks. [9]

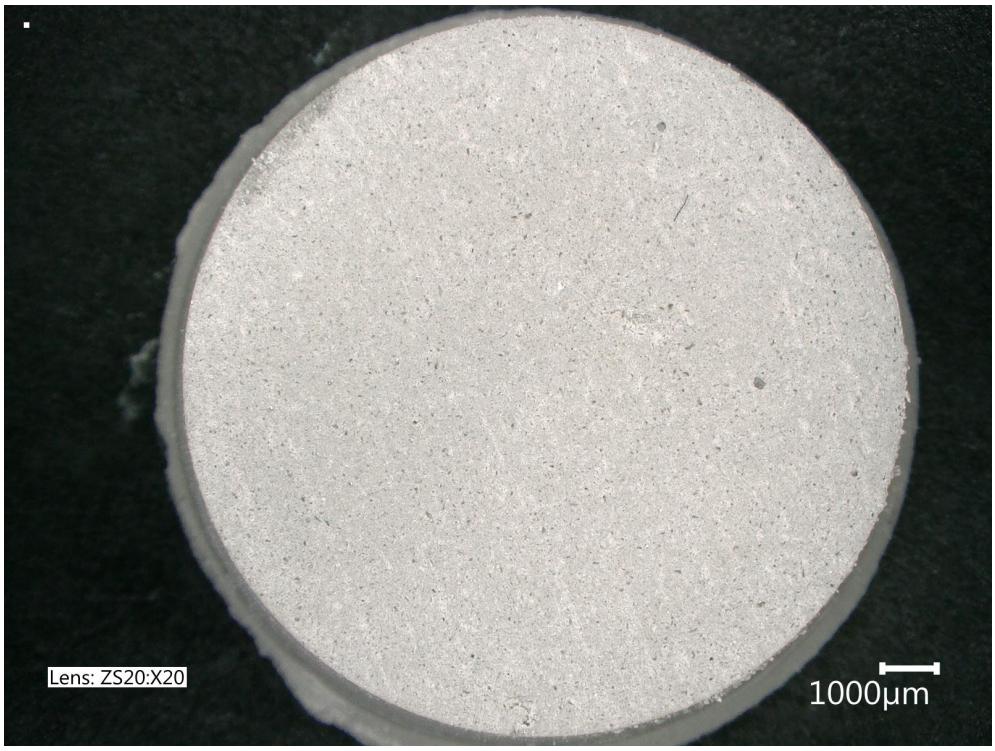

Figure 22 Vacuum Degassed Sample of 40 Volume Percent Filler Polymer Composite

Once a high quality, void free, samples were able to be produced, samples for testing in laser flash and DSC analysis could be produced. In order to maintain a high degree of thermal coupling between the conductive filler particles and the polymer matrix, drying of the filler material was completed to remove any moisture content as moisture can have adverse effects on the polymer-particle interface [48]. To remove moisture of the filler material, the conductive powders were heated at 100°C for 6 hours before being mixed into the epoxy matrix.

Thermal Conductivity of Polymer Composite

The thermal conductivities were determined using a modified version of the thermal diffusivity equation. Using experimental methods, the unknown variables in the equation can be determined. Once these variables are determined, a simple calculation can be completed to determine the thermal conductivity of the polymer composite. The modified thermal diffusivity equation is as follows:

$$\kappa = \alpha \rho C_p$$

Where α is the thermal diffusivity, ρ is the density and C_p is the specific heat capacity. To measure these values, laser flash analysis, and DSC tests were completed to determine the thermal diffusivity and specific heat capacity of the polymer composite respectively. The density of the material was determined through mass and volume measurements of the tested samples.

Laser Flash Analysis for Thermal Diffusivity

Thermal diffusivity of a material is known as a materials ability to conduct thermal energy relative to its ability to store thermal energy and is measured in $\frac{m^2}{s}$. This material property is measured through the laser flash analysis (LFA) method. This method is conducted by applying a thermal energy source, a laser, on one side of a flat, cylindrical disk. The heat rise on the opposite side of the disk is measured as a function of time, this allows for the determination of thermal diffusivity [49]. The LFA testing completed to determine values for the thermal diffusivity of the developed polymer composites was in compliance with ASTM E1461 and ASTM

E2585 [50], [51]. Laser flash analysis was conducted on a NETZSCH LFA 457 MicroFlash thermal diffusivity tester. Accuracy of the device is within ±5% for most materials [52].

Differential Scanning Calorimetry for Specific Heat Capacity

The specific heat capacity is the ability that a material has to store thermal energy. It has the units of $\frac{J}{kgK}$, that is the amount of energy required to raise a kilogram of material by one Kelvin. The Differential Scanning Calorimetry (DSC) method is used to measure specific heat capacity, which compares the thermal energy applied to a sample to a reference material. Using precise measurements of heat flow and temperature measurements, the specific heat capacity of the sample can be determined. Practices and methods used for the DSC testing for the polymer composites conforms to ASTM E1269 [53].

Thermal Conductivity Predictions

Given the materials that have been selected as candidates for the polymer composite potting compound, it is possible to estimate the thermal conductivity at different filler percentages. Figure 23 displays the expected trend for thermal conductivity of a polymer that has hexagonal boron nitride or aluminum nitride as filler materials. It was determined earlier that 25 volume percent filler is the maximum possible filler percentage that is vacuum infusible, however higher volume fraction composite samples could be produced through compression molding. The higher filler percentage samples were created so that a trend could be developed with the

predictive Nielsen model. In order to make predictions on the thermal conductivity of the polymer composites, certain assumptions needed to be made on the geometry and packing factor of the filler materials. The value for "A" in the Nielsen equations was assumed to be 2.08 for the small flake HBN and 1.5 for the spherical AlN particles. An equal packing factor of 0.601 was assumed for the two filler materials.

Table 11 Constants Used for Thermal Conductivity Predictions

	Thermal Conductivity (W/mK)	A	Φ_m
Elan Cast	0.82	N/A	N/A
HBN	600	2.08	0.601
AlN	180	1.5	0.601

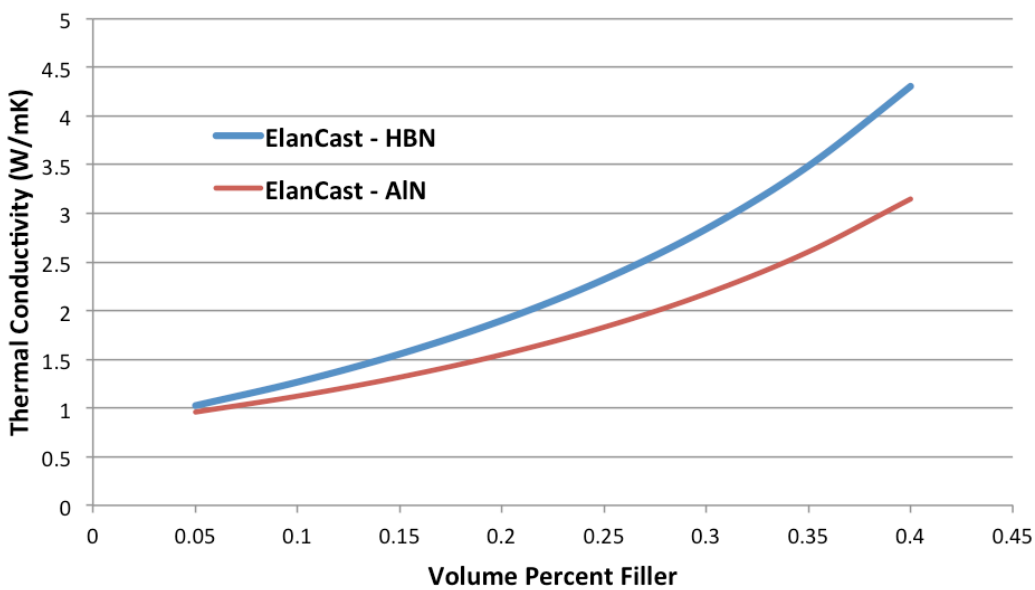

Figure 23 Thermal Conductivity Prediction of ElanCast Polymer with AlN and HBN Filler

Results of Thermal Conductivity Analysis

After what was learned from the implementation tests for different sized filler materials, it was determined that small particle sizes of both AlN and HBN would be tested for thermal conductivity. For both HBN and AlN composites, particle sizes on the order of 5μm were used. Figure 24 displays a comparative analysis between an ElanCast polymer filled with 10 volume percent HBN and AlN. Completing this study would allow a decision to be made on which particle should be used for the final polymer o be implemented into the motor stator. This test was completed at 10 volume percent filler since that was the maximum possible filler amount before the HBN filled epoxy became too viscous for vacuum infusion.

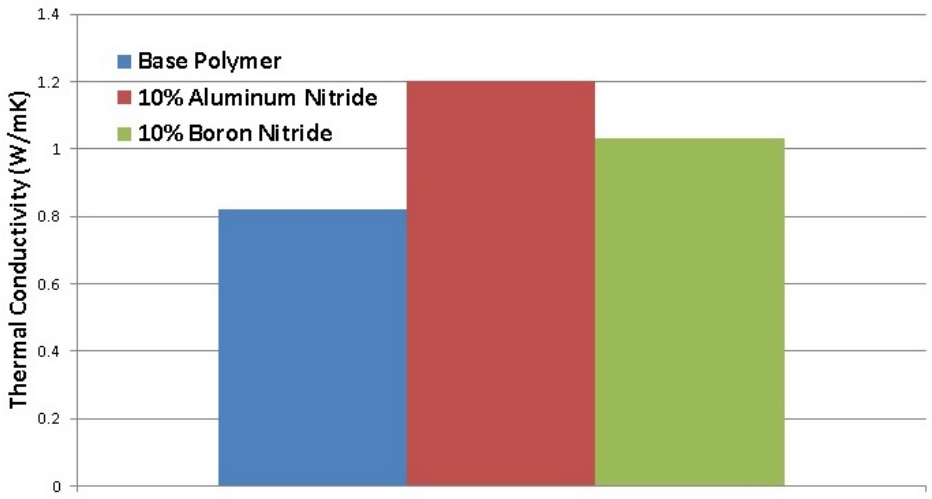

Figure 24 Comparison of 10 vol% HBN and AlN in Elan Cast P300 Polymer

These results conflict what is predicted using the Nielsen model since boron nitride has a greater intrinsic thermal conductivity than aluminum nitride. Since the intrinsic thermal conductivity is of HBN is greater than AlN, the cause of the lower than expected results may be caused by particle-matrix interaction or the

anisotropic behaviour of hexagonal boron nitride. Since the hexagonal boron nitride particles are flake shaped, the maximum thermal conductivity of 600W/mK is only possible in the in-plane direction. In the through plane direction, HBN has a significantly lower thermal conductivity of 30W/mK. Other studied completed on thermally conductive polymer composites stated values of 121 and 71W/mK for the in-plane and through-plane conductivity of HBN [15]. This could be a considerable source of error in predicting the thermal conductivities of the polymer composites. Since HBN exhibits this anisotropic thermal behaviour, the thermal conductivity might vary depending on which direction measurements are being taken. Figure 25 displays the variation of orientation of HBN flakes in an epoxy matrix.

Figure 25 Arrangement of HBN Flakes in Polymer Matrix

It can be clearly seen that some particles are lying flat and appear as having a large surface area. Other particles look as if they are long and thin in geometry; however this is simply due to the orientation that the particles are being viewed at. The long and thin particles seen in Figure 25 are actually HBN particles that are in a vertical orientation. This greatly affects thermal conductivity as the orientation in which the particles are arranged could have an incredible effect on thermal conductivity in measured direction. Works have been completed on using magnetic fields to orientate HBN particles within a matrix material to improve thermal conductivity [14].

Since the final operation of the polymer composite is within a motor stator, the use of magnetic field alignment of filler particles is unfeasible. Since the motor stator is a complex geometry, there is a number of direction in which heat flow occurs. For this reason, it is necessary that the produced polymer composite has isotropic thermal transport properties. Additionally, in order to achieve aligned HBN particles, the addition of iron particles is required to align the HBN particles to the applied magnetic field [14]. This makes this method very unattractive for use within an electric motor because the iron particles would have a negative effect on the motor's flux path and may also generate losses when exposed to an alternating magnetic field.

Given the initial results of low filler percentage polymer composites, it was determined that higher thermal conductivity polymer composites could be produced by using AlN as a filler material instead of HBN. Due to the anisotropic

behaviour of HBN, it was determined that a material with equal thermal conductivity in all directions is required for use within a motor stator. More testing samples were created using ElanCast P300 as a matrix material and varying amounts of AlN as filler material.

Since the environment within electric motor is not at constant temperature, the polymers were tested throughout a temperature range from 30°C to 180°C. This was done to better understand polymer thermal properties at elevated temperatures. Figure 26 presents the results from the thermal testing that was completed on samples of ElanCast P300 polymer with varying amount of aluminum nitride filler.

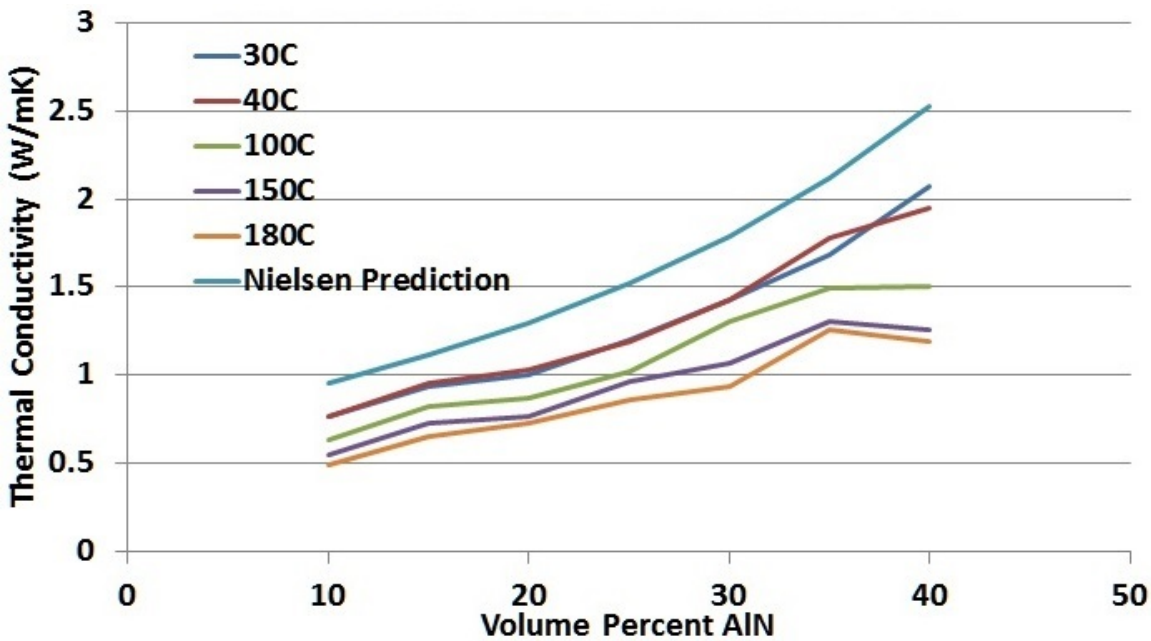

Figure 26 Comparison of Attained Experimental Thermal Data to Nielsen Model

It can be seen in Figure 26 that as the tested sample temperature increased the polymer composites ability transfer heat decreased. Although the measured thermal conductivities are lower than the expected values, these exists a similar trend between the predicted and actual results. It is evident from the Figure 26. Both tests

completed at 30°C and 40°C have very similar results, with the 40°C sample differing slightly at very high filler percentages. The data obtained for the higher temperature tests, however, have significant differences in trend when compared to the Nielsen model. These inconsistencies may be attributed to a number of factors that were assumed in predicting the thermal conductivity values. Any error made in estimating the "A" value or maximum filler packing factor would results in an error in the prediction. Additionally, imperfect sample preparation could cause the discrepancy in the results.

Through the testing of the polymer composites created using AlN in an ElanCast P300 matrix, it was possible to create a sample that had a maximum thermal conductivity of 2 W/mK. This value is over 250% more than that of the base polymer. When considering the implementation of the polymer, the maximum possible thermal conductivity is 1.25W/mK. This was achieved by the sample with 25 volume percent AlN.

5. Thermal Modeling Development and Analysis

Based off of the one dimension thermal analysis completed in the introduction, axial motor cooling seems to have potential to improve the amount of thermal energy that can be removed from an electric motor. One-dimensional analysis is a useful tool for proving the concept of axial cooling; however it is not accurate for quantifying the performance increase attributed to the implementation of axial cooling. To gain a better understanding of the heat transfer and local temperatures within an electric motor, a more complex 3 dimensional finite element model was created. By utilizing ANSYS and its CFX solver, a full thermal simulation of a baseline jacket cooled motor could be compared to the axial cooled motor design [54]. By using this software, important motor information such as peak temperatures, thermal gradients and heat flow can be determined. By comparing these metrics between the axial cooled and non-axial cooled motors, a quantifiable performance increase can be determined. Simulations completed for this work were evaluated at both steady state and transient conditions. In doing this, it is possible to determine the maximum possible continuous and peak operating power. The following section will discuss in detail the methods taken to set up the thermal model and will analyze the results. Both axial cooled and baseline jacket-cooled motors are investigated and a quantifiable performance increase is discussed.

Boundary Condition Definition

Interface Conditions

A major source of thermal resistance within an electric machine, and any conjugate heat transfer model for that matter, is the resistance associated with interfaces. This resistance is due to the imperfect surface contact between two interfacing surfaces. In the case of motor windings, this surface contact resistance is significant as the interfacial surface area between the windings and the stator is small. To overcome this interface resistance, motor stators can be encapsulated in an epoxy resin to achieve an improved surface contact between the motor coils and the surrounding components. For the finite element model developed for this study, this interface resistance between the coils and the surrounds components is considered to be small and is therefore negated as it can be assumed to have a negligible contribution to the overall thermal resistance experienced from the motor coil to the point of heat extraction.

Although the interface resistance of the coil-stator and coil-axial cooling channel interface is considered negligible, the interface resistance between the stator and the motor casing is not. Given that the motor stator and casing are both made of solid metallic material, there exists an interface resistance that is too great to be considered negligible. Thermal resistance from two mating solid surfaces is dictated by the surface roughness as well as the pressure applied to the contacting faces. By considering the contact with one another are steel and aluminum and they both

have general surface roughness and general pressure applied, the interface thermal resistance can be estimated from literature values. Using interface modeling in ANSYS CFX [54], this resistance is accommodated for by applying a conservative thermal resistance of 4000W/m^{2}K at the interface [55], [56].

Stator Slot Definition

Since modeling a complete motor with every small detail included, such as individual copper wires and coatings is incredible difficult, several assumptions were made in an effort to reduce computing power required to solve the simulation. Firstly, a ¼ scale motor was simulated with symmetry conditions applied to the quadrant surfaces. This reduced the number of elements and interfaces in the simulation to make it more manageable to solving while still maintaining the same model fidelity as a full motor simulation.

Previous studies determined a combined thermal conductivity of both the copper windings and the coating and treated the motor coils as a homogeneous solid with constant thermal conductivity [18], [57]. This approach was not taken for this study as the thermal conductivity of the infiltrating material, or potting compound, is greater than those used in the mentioned studies. By applying the appropriate boundary conditions and modeling the individual copper windings of the motor, an improved assessment of the heat flow from the coils can be determined. The motor windings were modeled as 3mm in diameter, rather than the diameter of an AWG 13 wire, which is 1.828mm. This was done to reduce the number of interface conditions

between the coils and stator, which consume a considerable amount of computing resources. Coil coating thickness was accounted for by applying an interface condition around the coils that has a thickness of 0.1mm and a thermal conductivity of 0.2W/mK. For both cooling designs, the motor coils were modeled to be infiltrated in the developed thermally conductive potting material. The materials used to pot the motor coils is assumed to be a homogeneous material with a bulk conductivity of 2W/mK. The value of the thermal conductivity of the polymer-potting compound is somewhat irrelevant as this is a comparative study. Since the goal is to directly compare a non-axial cooled motor to an axially cooled motor, any error in the assumption of the thermal conductivity will be relative to each cooling design.

Heat Generation

Heat was introduced into the system by way of volumetric heat generation from the coils and the stator and a surface heat flux input on the interior surface of the stator. The heat flux boundary condition was applied to capture the heat transferred from the rotor to the stator. A "worst case scenario" case is assumed where 100% of the heat generated by the rotor is transferred into the stator.

The value of heat applied to the motor depends on the power rating and efficiency of the motor itself. For this study, it was assumed that the hypothetical motor to be analyzed was operating at an efficiency of 90%. For example, if the motor it able to operate at 200kW, 20kW would be inputted into the thermal system as coil, stator

and rotor losses. Since only ¼ of the motor is being simulated, the amount of power being inputted into the motor is divided by 4. In the 200kW motor example, only 5kW of heat would be inputted into the system in various locations.

The thermal energy generated through losses occurs from different sources of the motor. The three major sources considered for the thermal simulations are the copper losses, stator losses and the rotor losses. Depending on the electromagnetic, geometric and material design of the motor, the percentage of these losses can vary. Given a hypothetical motor design, the percent share of the total losses can be distributed between the copper, stator and rotor inefficiencies. The total losses of the motor are assumed to be generated through 35% for copper losses, 32% for Stator Losses, 14% for rotor losses and 19% for frictional and stray losses. Frictional and stray losses are not considered for the thermal analysis as these losses are assumed to have negligible effect on the coil and stator temperatures.

As described in the introduction to motor losses in Chapter 2, the copper losses are rarely equally distributed over the cross section of the coil. With additional copper losses being generated from flux leakage at the stator tooth tip, the copper coils near the stator tip have higher losses than the coils located at the base of the stator tooth.

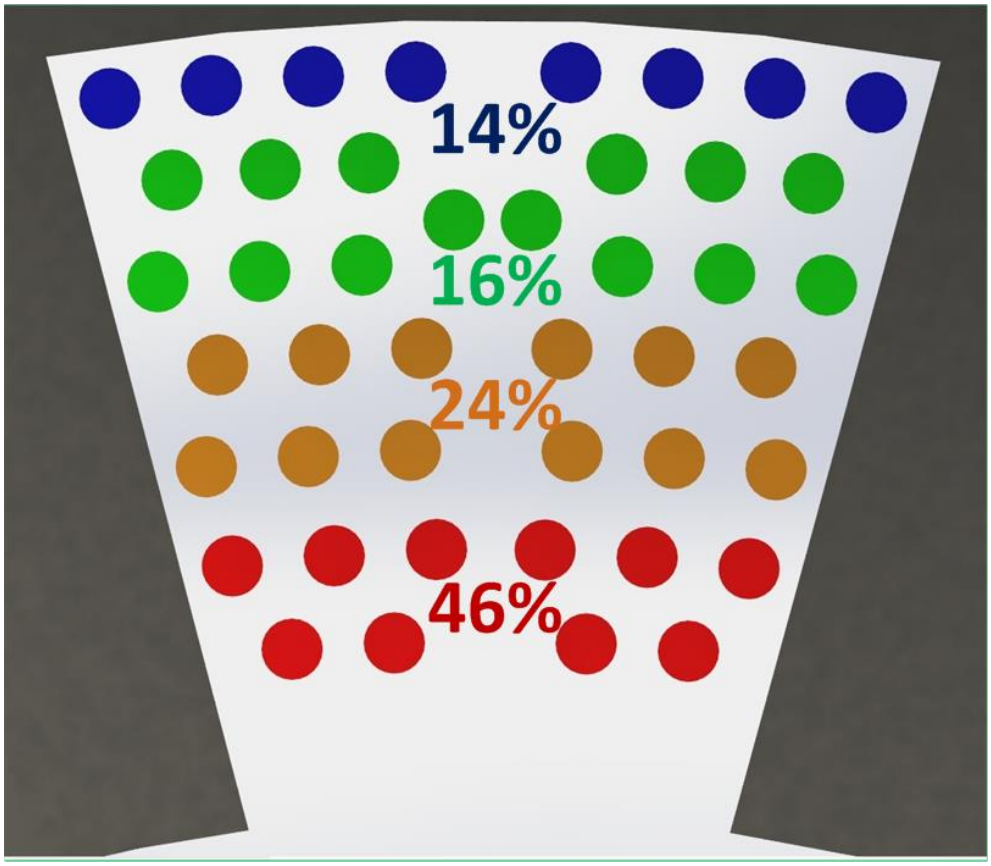

Figure 27 Coil Loss Distribution

Figure 27 displays the distribution of copper losses within the stator slot. Coils near the stator tip account for 46% of the copper losses, whereas the percent share of the copper losses decreases as you move away from the stator tip.

Heat Evacuation

Thermal energy of the models was removed through liquid cooling channel flowing in between the stator slots as well as a "snake" channel flowing through the motor casing. The turbulent flow model used to calculate the fluid dynamics within the cooling channels was the k-ε model, which is a very popular model for interior flow. By paying particular attention to the boundary layer effect of fluids, inflation-

meshing conditions were applied to ensure proper mesh resolution in this sensitive area. Fluid dynamic analysis was completed since the heat transfer coefficient for the "snake" cooling channel in the motor casing would be very difficult to determine. It was decided that less error would be introduced into the simulation if the fluid dynamics were calculated through finite element methods rather than estimated. Inlet boundary conditions were water at 25°C at a mass flow rate of 0.32 liters per second for the frame channel and 0.25 liters per second for each of the three axial cooling channels. In automotive applications, the coolant temperature is typically in the range of 60°C. The effect of the coolant temperature on peak motor temperature will be discussed in the sensitivity analysis. An inlet turbulence intensity of 5% was applied to model any upstream turbulence generation in the cooling channels.

Thermal Model Mesh

Thermal and fluid simulations are completed through calculations of heat transfer and fluid momentum and turbulence across a number of different measuring points. These measurement points, known as nodes, are where calculations are completed to properly model the thermal gradients and fluid dynamics of the system. Without a high quality mesh, the accuracy of the simulation can be compromised [58].

In order to effectively capture the heat transfer and fluid dynamics of the simulation, several meshing conditions were applied to different surfaces of the motor. Table 12 summarizes the mesh size for the different bodies in an axial cooled motor simulation. The meshing conditions for the baseline motor simulations are identical

to those stated in Table 12; however the axial cooling channel and axial water bodies are not included.

Table 12 Meshing Conditions

Location	Element Type	Mesh Size (mm)
Coils	Tetragonal	1
Polymer Potting Compound	Hexagonal	1
Axial Channel	Tetragonal	1
Axial Water	Tetragonal	1
Stator	Tetragonal	7
Casing	Tetragonal	7
Frame Water	Tetragonal	7

The mesh sizes were selected based off of the size of the bodies to be meshed. Since the bodies existing within the stator slot have small distances between them and small radius corners, a fine element size was applied. Bodies such as the stator and the motor casing and frame water are large bodies, where a lower mesh density can be used.

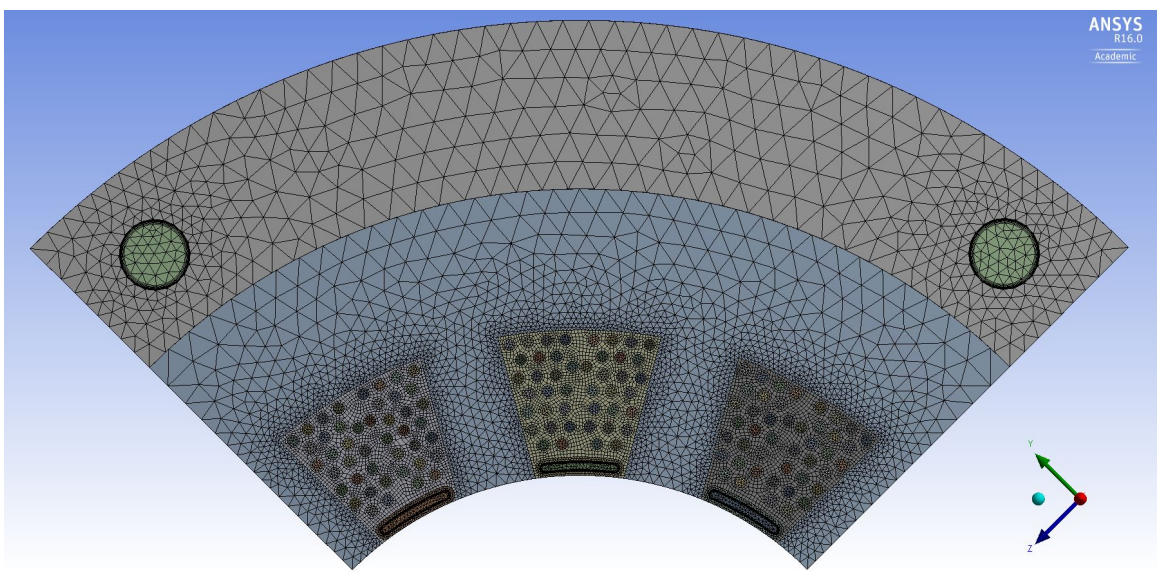

Figure 28 Overall Motor Mesh

Figure 28 displays the final mesh that was used for all thermal simulations of the axial cooled motor. In order to achieve model integrity, it is important to maintain a roughly equal element density on either side of interfacing surfaces. For example, the polymer potting compound and the stator were meshed as separate bodies with an interfacing surface on the inside of the stator slot. In order to reduce the amount of error in data transfer through the interface, the mesh density on either side of the interface must be relatively close. This reduced the need for data interpolation in between the nodes on either side of the interface. To achieve this, mesh refinement conditions were applied on proximity and curvature for the stator to taper down the mesh size from 7mm to 1mm near the stator slot surface. Figure 29 displays the how the element size reduces as it nears the stator slot surfaces.

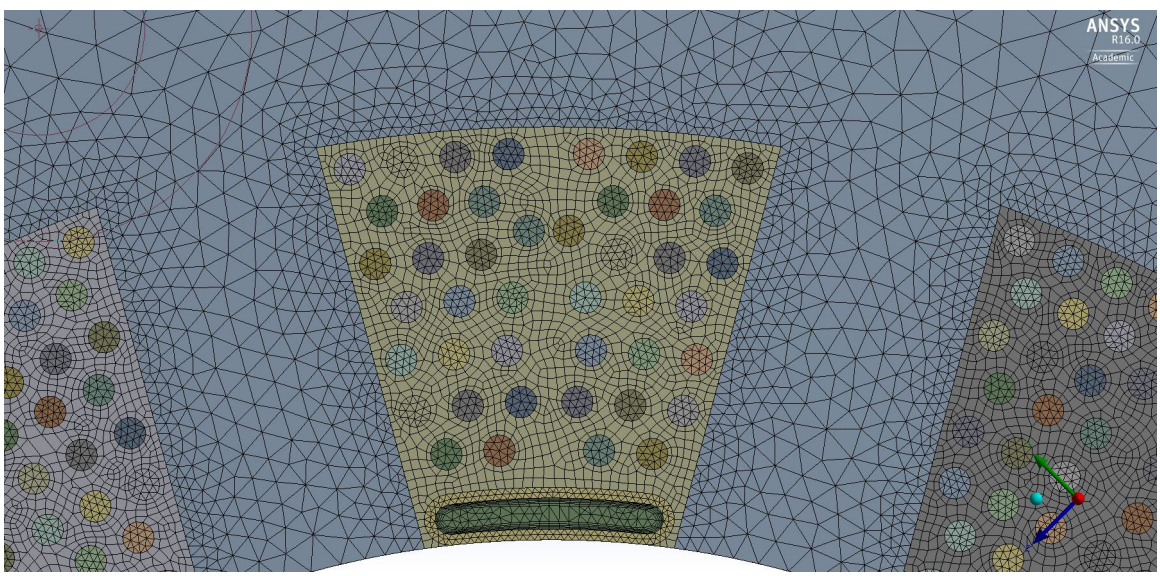

Figure 29 Stator Slot Meshing

Since fluid dynamics are being calculated in both the axial cooling channel and the frame cooing channel, it is necessary to apply inflation layers to model the boundary

layer effect of fluids passing near walls. Inflation layers are specialized elements that start very small and increase in size as you move away from a surface. This meshing method helps to increase the accuracy of the calculated fluid dynamics within the cooling fluids. The final mesh consists of 6.3 million elements and 2.4 million nodes. This mesh density is of high enough quality to calculate the heat transfer and fluid dynamics of the thermal simulation.

Quantifying Performance Increase

Given the input boundary condition listed, both the baseline motor and the axially cooled motor will experience a temperature increase. Depending on the two designs' abilities to dissipate thermal energy out of the system, the amount of temperature rise during steady state condition will change. Since the motor is considered an H-class motor, the maximum temperature possible in the critical motor components is 180°C, or 453K. Critical motor components are considered to be the motors coils and the polymer potting compound, both of which are rated to H-Class Specifications.

Given that axial cooling has the potential to reduce the internal temperature of a motor, it was estimated that peak motor output power could be increased without an increase in the temperature of critical motor components. To determine the amount of thermal energy that the baseline and axial cooled motor designs can dissipate, a number of simulations were completed at different motor output powers. Values for heat input were determined by assuming a 90% motor efficiency

and then distributing the amount of losses to the coils, stator and rotor depending on their respective percent share of the total losses. Several motor simulations were completed at increasing input powers while monitoring peak motor temperature. Once a simulation was completed in which the coils and potting material achieved a peak temperature within 5°C of its maximum operating temperature, this was considered the max power achieved by that cooling design.

Baseline Motor Simulation Results

Given the methods used to determine maximum operating power of a cooling design, the peak power of a baseline motor was determined to be 90kW. Table 13 and Table 14 show the calculations of input power for the various inefficiencies of the 90kW motor.

Table 13 90 kW Baseline Motor Loss Calculations

Continuous Motor Power	90	kW
Efficiency	90	%
Total Thermal Power	9	kW
For 1/4 Motor	2.25	kW
	Percent of Total Losses	Power Input (kW)
Copper Losses	35	0.788
Rotor Losses	14	0.315
Stator Losses	32	0.720

Table 14 Copper Loss Distribution for 90kW Baseline Motor

Copper Losses	Power Input (kW)
14%	0.110
16%	0.126
24%	0.189
46%	0.362

A baseline jacket cooled motor design was simulated given the initial boundary conditions described in the previous section. The baseline and axial cooled simulations are identical in their setup with on the only exception being that the baseline deign does not have an axial cooling channel packaged. The motor coils are assumed to be potted in a thermally conductive polymer composite.

The temperature contour plot generated through simulation was as expected when considering the one dimensional thermal resistance calculation from the introduction. Since the point of heat evacuation is around the circumference of the motor, the point of highest thermal resistance, and thus the point of greatest temperature was estimated to be at the centerline of the stator slot. The thermal analysis confirmed this hypothesis with the thermal gradient clearly showing that the further you get from the cooling jacket, the greater the temperature is.

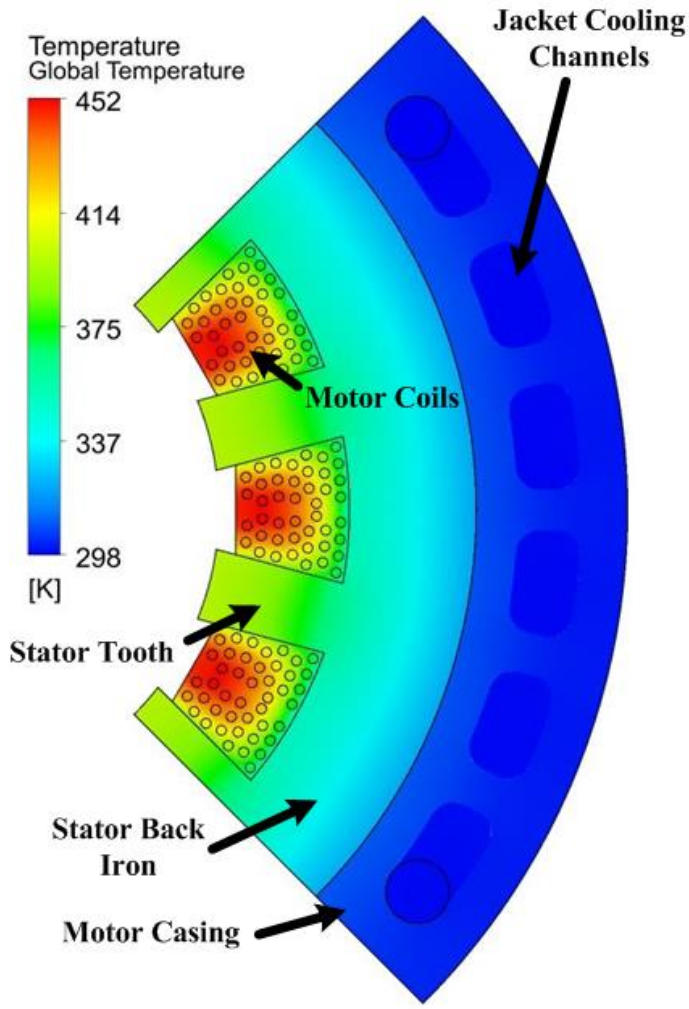

Figure 30 Temperature Gradient of Baseline Motor at 90kW

From Figure 30, it can be seen that the point of peak temperature is evident to be within the coil that is closest to the centerline of the stator slot, and closest to the inner surface of the stator.

Table 15 Peak and Average Temperatures for Baseline Motor

90kW	Peak Temp (°C)	Average Temp (°C)
Stator	122.6	65.7
Polymer	180.3	136.6
Coils	180.5	138.4

Considering what has been learned from the thermal simulation of a jacket cooled motor, it helps to justify the implementation of axial cooling channels within a stator. Not only will the axial cooling channels be removing additional thermal energy from the stator and coils, but they will also be cooling the most critical and hottest portion of the motor.

Axially Cooled Motor Simulation Results

The simulation for the case of the motor with the axial cooling design implemented was set up in an identical manor as the baseline simulation. For consistency, identical boundary conditions were used with the only difference in the model being the addition of the axial cooling channel. Again, a thermally conductive polymer-potting compound with a thermal conductivity of 2W/mK was used as an infiltration material for the motor coil.

Table 16 150kW Axially Cooled Motor Loss Calculations

Continuous Motor Power	150	kW
Efficiency	90	%
Total Thermal Power	15	kW
For 1/4 Motor	3.75	kW
	Percent of Total	Power input (kW)
Copper Losses	35	1.313
Rotor Losses	14	0.525
Stator Losses	32	1.2

An identical procedure was used to determine maximum motor output power that the thermal design is capable of achieving. Heat input parameters were continuously increased until the peak motor temperature was within 5 degrees of 180°C. For the

axially cooled design, the maximum motor temperature was observed at a motor output power of 150kW. The heat input powers for a motor output power of 150kW can be seen in Table 16.

Table 17 Copper Loss Distribution for 150kW Axially Cooled Motor

Percentage Copper Losses	Power Input (kW)
14%	0.184
16%	0.210
24%	0.315
46%	0.604

Figure 31 displays the thermal gradient of an axial cooled motor that is operating at a continuous power output of 150kW. Since motor output increases by 60kW, it is clear that the implementation of axial cooling channels make a significant increase in overall cooling of the motor. Not only is motor power increased with no increase in coil peak motor temperature, but the average temperatures of all critical motor components is also lower than the baseline motor design operating a maximum possible output power.

Table 18 Peak and Average Temperatures for Axially Cooled Motor

90kW	Peak Temp (°C)	Average Temp (°C)
Stator	94.1	67.5
Polymer	173.8	121.1
Coils	176.1	131.8

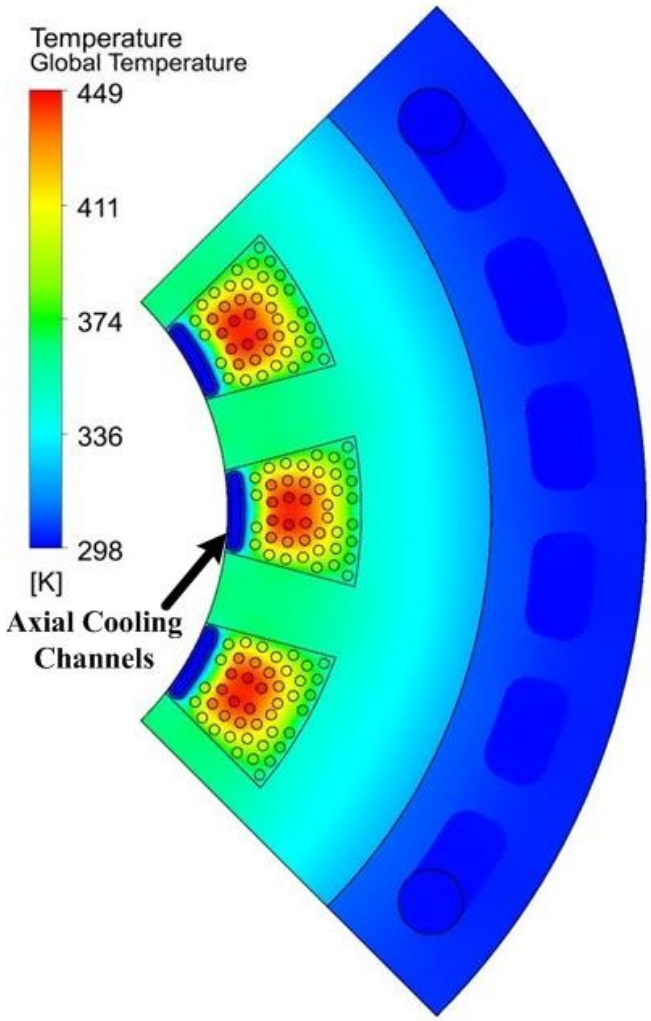

Figure 31 Temperature Gradient of 150kW Axial Cooled Motor

Comparative Analysis of 90kW Axial and Non-Axial Cooled Motors

Since the thermal analysis of the baseline and axial cooled motors were completed at different thermal energy inputs, it is difficult to directly compare their temperature gradients. To better understand the effectiveness of axial cooling relative to a non-axial cooled motor, an analysis was completed between the two cooling designs with the same heat input. In order to directly compare the thermal

gradients of the two designs, a corrected temperature scale was used to compare the temperature gradients of the simulations.

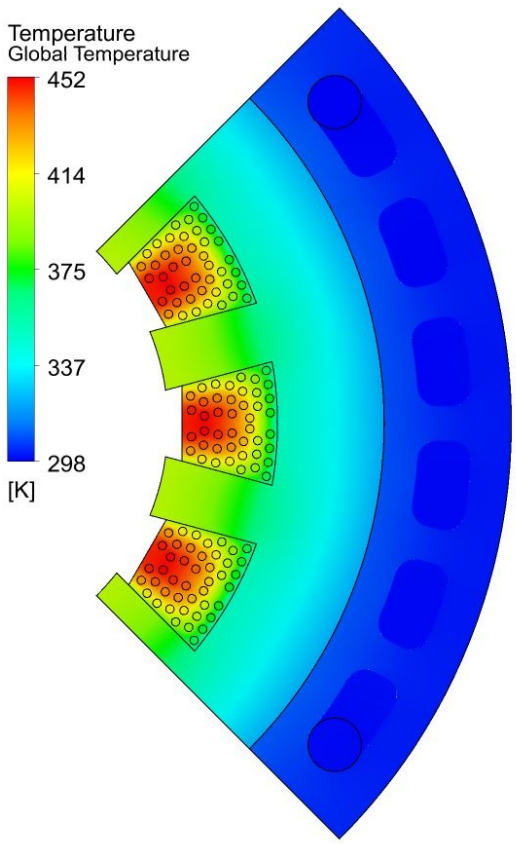

Figure 32 90kW Baseline Cooled Motor

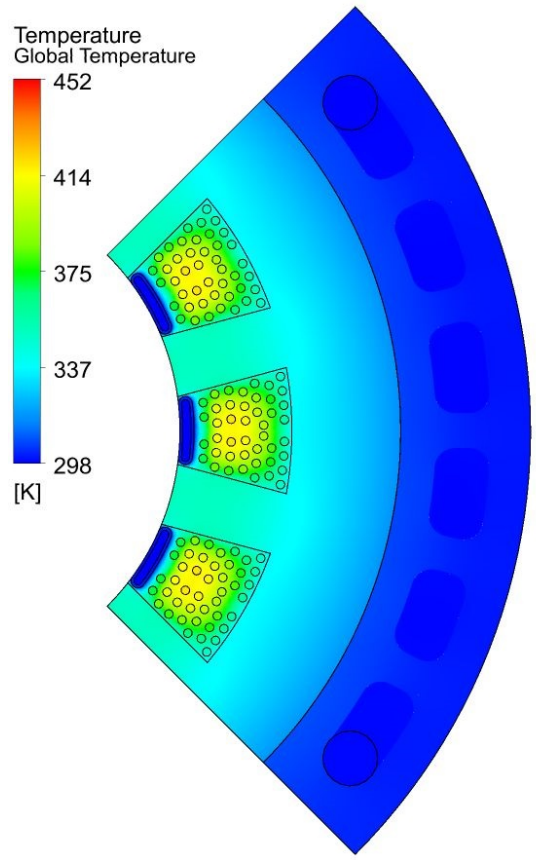

Figure 33 90kW Axially Cooled Motor

As seen in Figure 32 and Figure 33, the comparative temperature profile between the 90kW baseline motor and the 90kW axial cooled motor is quite significant. Peak temperature in the axial cooled motor is 146°C, 35°C cooler than that of the baseline motor cooling design.

Table 19 Peak and Average Temperatures of Baseline and Axially Cooled Motors

	Baseline Motor		Axial Cooled Motor	
90kW	Peak Temp (°C)	Average Temp (°C)	Peak Temp (°C)	Average Temp (°C)
Stator	122.6	65.7	80.2	58.8

Polymer	180.3	136.6	143.8	101.8
Coils	180.5	138.4	145.8	111.2

As expected, the tip of the stator tooth was expected to be the point of greatest temperature in the baseline cooling design. By looking at the thermal gradient of the stator of the two cooling designs, it is evident that the axial cooling moves the peak stator temperature away from the stator tip and towards the middle of the stator tooth.

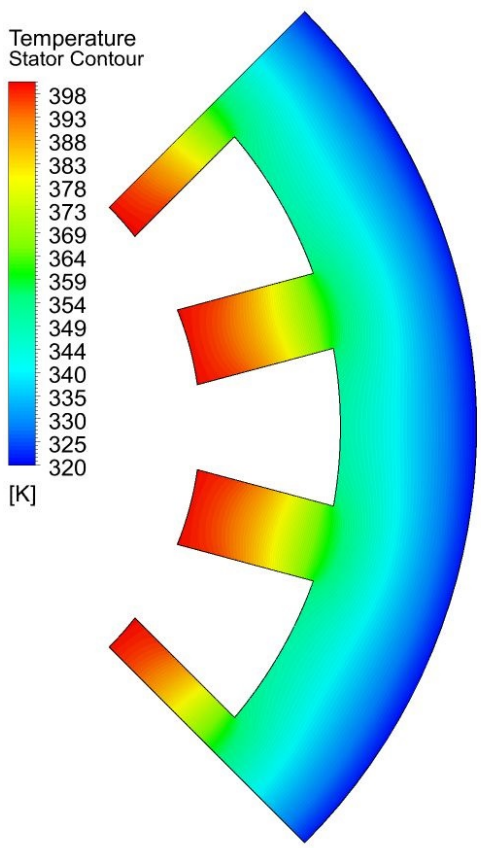

Figure 34 90kW Baseline Cooled Stator

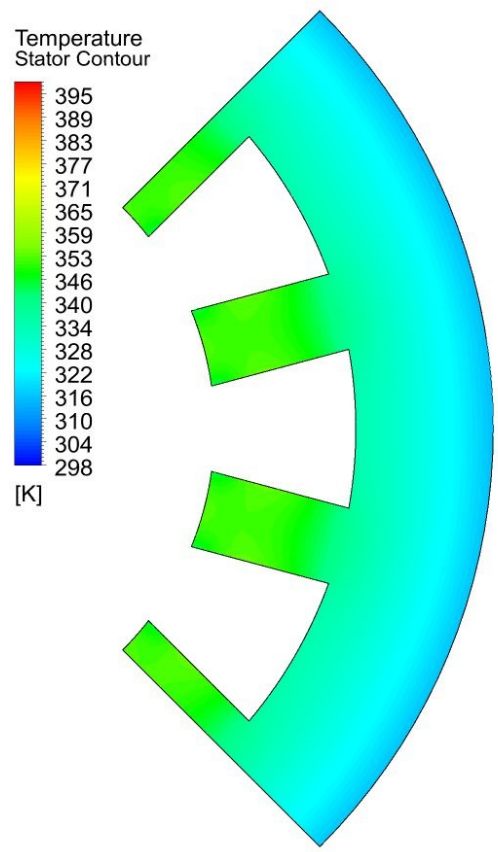

Figure 35 90kW Axially Cooled Stator Contour

In order to properly capture the effect that axial cooling has on the stator temperature, the two images are plotted on similar temperature scales. Peak stator

temperature of the baseline design is 138°C compared to the peak temperature of the axially cooled motor of 80.3°C.

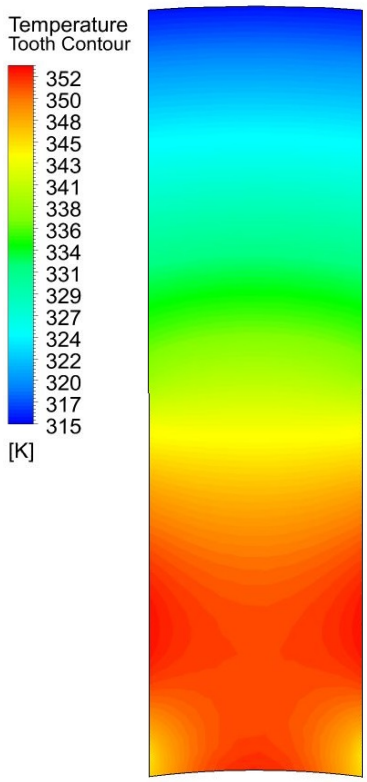

Figure 36 90kW Axial Cooled Stator Tooth Temperature Gradient

Not only does the axial cooled motor have a lower peak and average temperature when compared to the non-axial cooled motor, but the peak temperature in the stator is also at a different location. In the baseline motor, the maximum stator temperature occurs at the tip of the stator tooth. This is expected, as the tip of the stator tooth is the point of highest thermal resistance in the stator in a jacket-cooled motor. In the axial cooled motor, thermal energy is removed from the tip of the stator tooth, cooling the hottest point of the stator. Figure 36 shows the temperature gradient along the stator tooth of the axial cooled motor.

Figure 37 displays the stator tooth temperature gradient of the two analyzed cooling designs. Conversely to the jacket cooled design, the peak temperature in the axially cooled stator is not at the tip of the stator tooth. Rather, the axial cooled motor has its peak stator temperature about 16m from the tip of the stator tooth. Figure 37 displays the temperature gradient along the stator tooth at the centerline as well as along the tooth edge. The distance of 0mm in the graph below is the tip of the stator tooth and the increased displacement is towards to back iron of the stator.

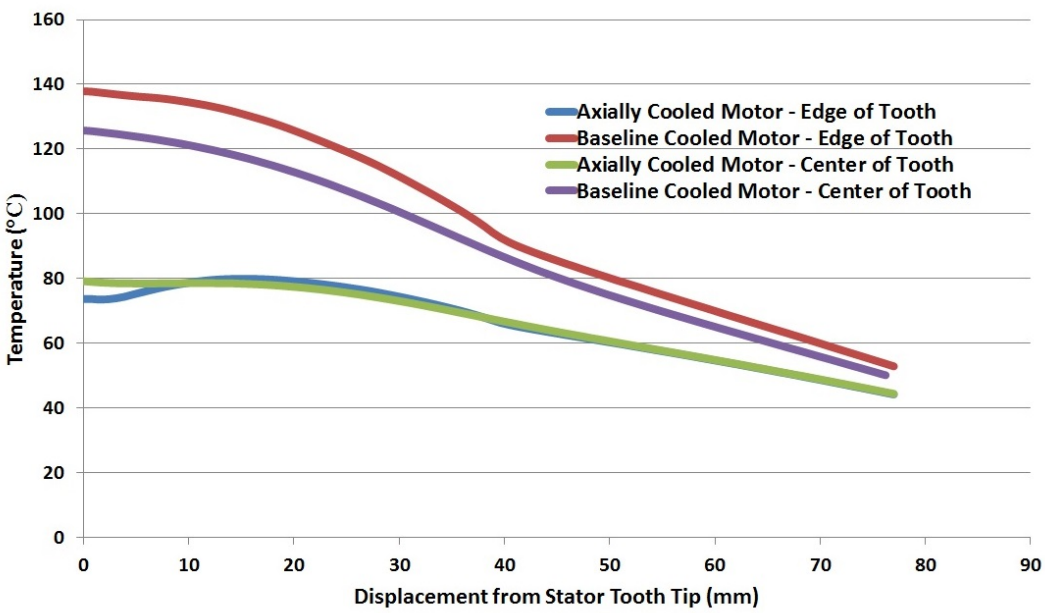

Figure 37 Stator Tooth Temperature Gradient

Another important area of the motor in which temperature is of great concern is within the stator slot where the coils and the polymer composite exist. The main goal of axial cooling is to reduce the temperature within the stator slot so that a higher current density can be achieved in the coils without a rise in temperature.

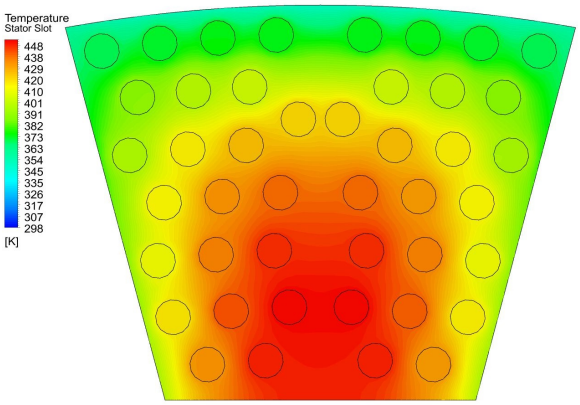

Figure 38 Baseline Motor Stator Slot Temperature Gradient

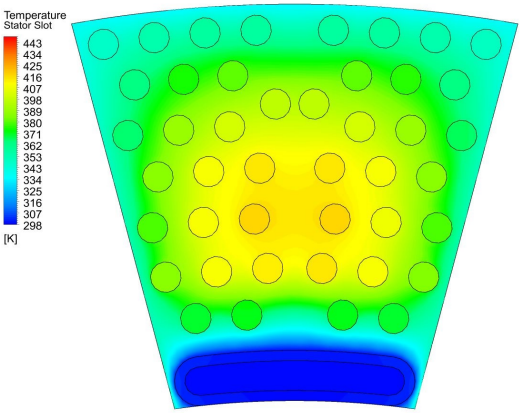

Figure 39 Axial Cooled Motor Stator Slot Temperature Gradient

Both temperature gradients are plotted on the same scale in order to effectively compare the temperatures. From Figure 38 and Figure 39, it is clear to see that the addition of an axial cooling channel drastically reduces the overall temperature of the stator slot, and thus the motor coils. With peak coil temperature remaining 35°C cooler in the axial cooled motor, it is possible to extend the life of the coil insulation.

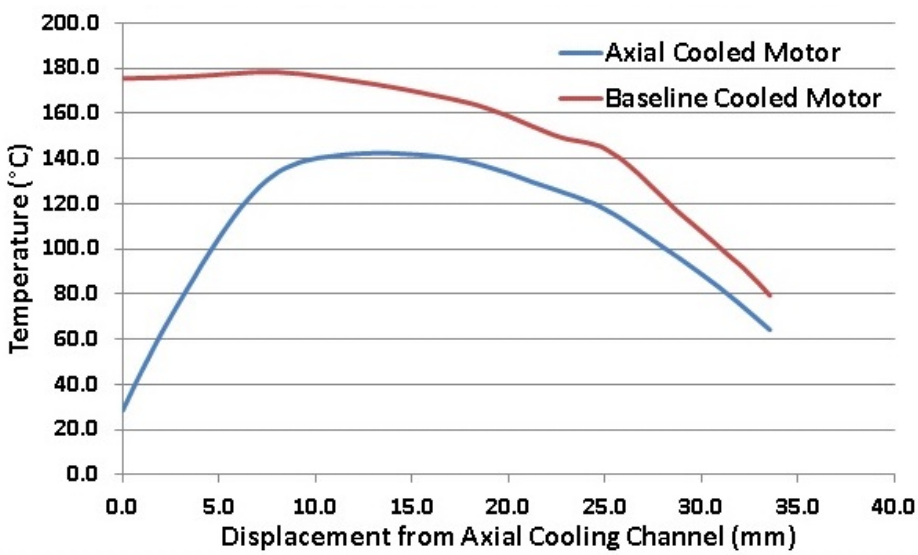

Figure 40 Midplane Stator Slot Temperature Gradient

Figure 40 displays the temperature gradient along the centerline of the stator slot. The effect of axial cooling can be clearly seen in the significant temperature drop towards the axial cooling channel.

Determination of Peak Motor Output Power

All previous thermal simulations of the two thermal management designs were completed in steady state conditions. This allows determination of maximum possible output power of an electric motor when considering the motor internal temperature rise due to losses generated within the stator, coils and rotor. Typically electric motors have two rated output powers, one continuous rating and one peak rating. The peak rating of the motor it a maximum output power that the motor is able to achieve during transient conditions. Assuming the motor is beginning at a temperature that is close to 25°C, the peak power rating would be a potential output power that the motor is capable of achieving as the temperature rises from 25°C to its maximum internal temperature of 180°C.

To determine peak motor power, simulations were completed for an electric motor with an output power of 225kW. Simulations were completed for a total time of 30 seconds in 3-second time steps. This allowed for good resolution of determining temperature rise in the motor as a function of time while still being able to complete enough time steps to experience a maximum motor temperature of 180°C, which is considered the thermal design limit.

Input power parameters were calculated just as they were in the previous steady state simulations and are shown in Table 20 and Table 21.

Table 20 225kW Axially Cooled Motor Loss Calculations

Continuous Motor Power	225	kW
Efficiency	90	%
Total Thermal Power	22.5	kW
For 1/4 Motor	5.625	kW
	Percent of Total Losses	Power Input (kW)
Copper Losses	35	1.97
Rotor Losses	14	0.79
Stator Losses	32	1.8

Table 21 Copper Loss Distribution for 225kW Axially Cooled Motor

Percentage Copper Losses	Power Input (kW)
14%	0.275
16%	0.315
24%	0.473
46%	0.906

The heat input values were held constant for all time steps to simulate an electric motor continuously operating at peak output power. Temperature data was collected at each time step so that a temperature rise in the motor could be plotted as a function of time.

Figure 41 displays the increase in peak temperature of the Coils, Polymers and Stator of an axial cooled motor. It is interesting to note that the peak temperature in the stator does not rise very much. After 30 seconds of transient operation, the difference in temperature between the coils and the stator is almost 120 °C where that difference is only about 80°C in the steady state case.

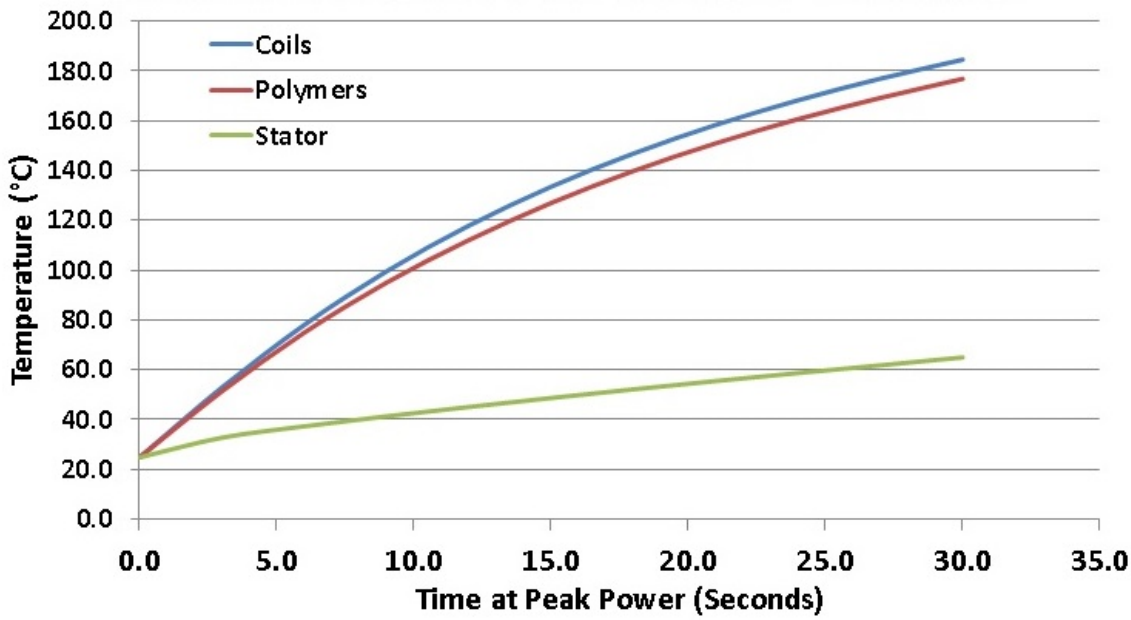

Figure 41 Transient Temperature Rise of 225kW Axial Cooled Electric Motor

The temperature gradient within the motor is significantly more drastic that that of the steady state simulations. Since the motor is only operating for a total of 30 seconds, the heat generated within the coils does not have time to conduct to the cooling channels. The short simulation time results in a much more concentrated temperature gradient that is located at the highest loss coils. Figure 42 displays the temperature gradient present in a 225kW electric motor after operating for 30 seconds.

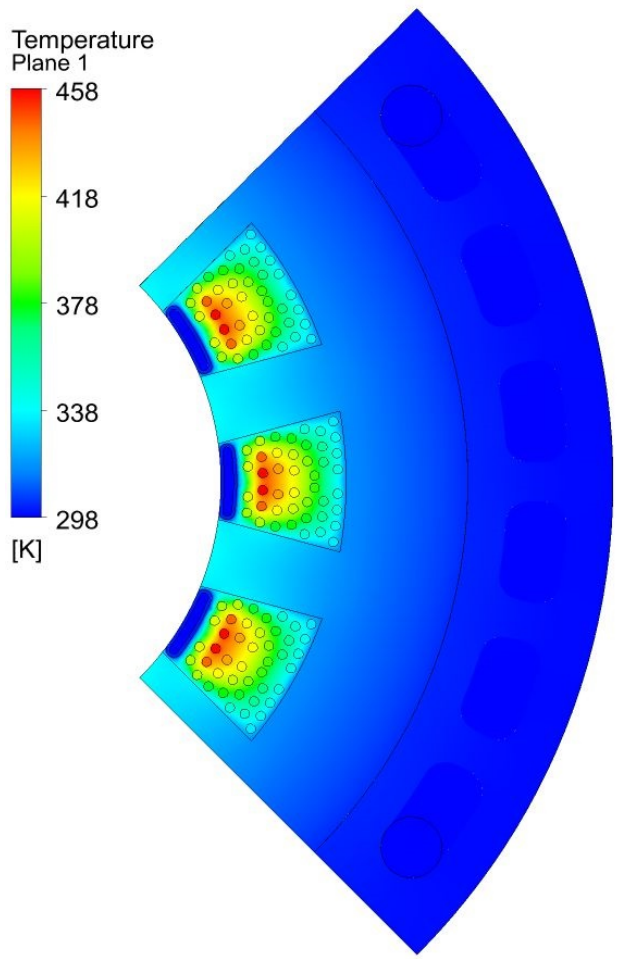

Figure 42 Temperature Gradient of 225kW Axially Cooled Motor at 30 Seconds of Operation

When comparing the temperature gradient of the transient case in Figure 42 to that of a steady state case in the previous section, it is clear that the generated thermal energy does not have time to conduct to the points of heat extraction. These results suggest that the temperature rise in a transient case of an electric motor is not necessarily dictated by the efficiency of its cooling system. The transient temperature rise is more dependent on other material properties such as specific heat capacity. Since every material requires a certain amount of energy to increase a certain mass by a certain temperature, this could result in axial cooling not having as

significant of an effect during transient operating when compared to steady state operation.

To compare the effect of axial cooling in a transient situation, the peak motor output power was determined for a baseline cooling design in transient operation and compared to an axial cooled design of equal input power. The peak motor output power for a baseline jacket cooled motor was determined to be 175kW for 30 seconds.

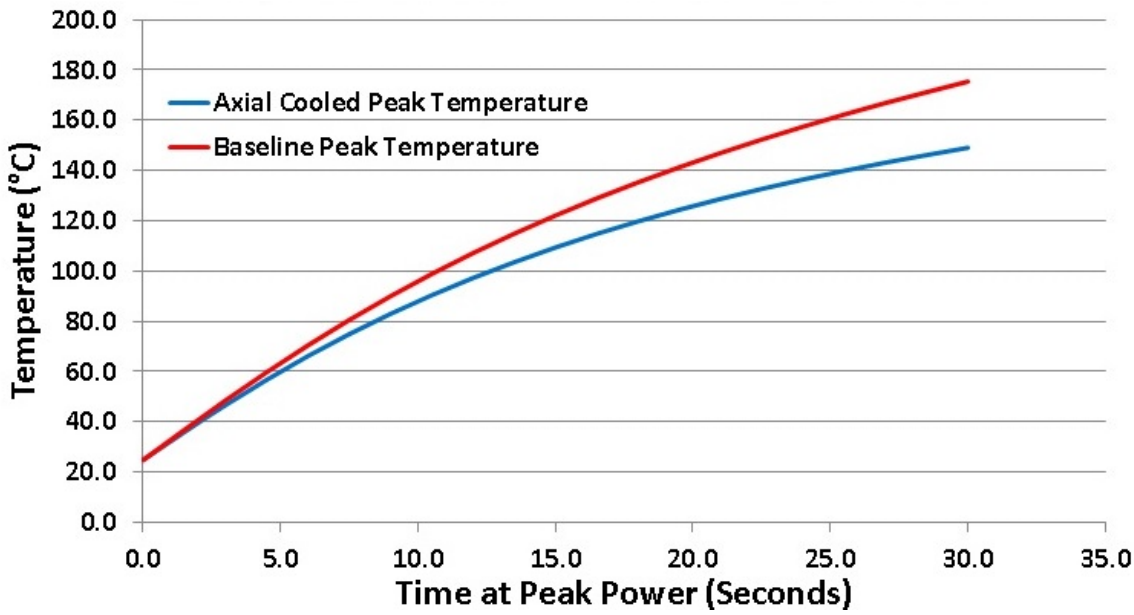

Figure 43 Peak Transient Motor Temperature of Axial Cooled and Baseline Motor Designs

Peak temperatures within the axial cooled motor are continuously lower than peak temperatures in the baseline motor throughout the entire 30-second cycle. At the 30 second mark of the transient analysis, the axial cooled motor has a peak temperature that is about 26°C cooler that the baseline motor.

Table 22 Peak Temperature after 30s of Peak Power Output

	Baseline	Axial Cooled
	Peak Temp (°C)	Peak Temp (°C)
Stator	66.1	56.8
Polymer	175.1	143.1
Coils	175.4	149.1

The difference in peak temperature in the transient case is not quite as dramatic as in the steady state case. However, it is clear that the axial cooling channel still have a considerable effect on the peak temperature within the motor. Furthermore, axial cooled motors are capable of increased power outputs in transient operation without an increase in peak motor temperature after 30 seconds of operation.

6. Sensitivity Analysis

Conducting a thermal analysis of an electric machine is a good way of estimating the ability of cooling design to dissipate heat from critical motor components. However, there is error associated with all measurements and assumptions that were used to create the thermal model. By considering these errors, it is possible to determine the upper and lower limits of the estimation. This creates a range of values that the thermal model is able to estimate when considering error in the system. Additionally, by adjusting thermal conductivity values of the thermally conductive potting compound, a trend can be developed that will can relate the max motor temperature, and thus the peak continuous motor output power, and the thermal conductivity of the polymer composite. This will allow future polymer development to estimate maximum possible motor power without the need to complete complex thermal simulations.

Parameters that can be adjusted to determine the systems sensitivity to their values are the thermal conductive of the polymer composite potting material, the thermal conductivity of the axial cooling channel, the interface resistance between the stator and frame, the interface resistance between the coils and polymer and the flow rate of fluid through the cooling channels.

To determine the models sensitivity, simulations were completed with varying values for each of the variables listed in Table 23. All simulations were completed assuming a 150kW axially cooled motor.

Table 23 Initial Values for Sensitivity Analysis

Variable	Value
Stator-Frame Interface Contact Resistance	4000 W/m²K
Thermal Conductivity of Polymer	2W/mK
Axial Channel Thermal Conductivity	20W/mK
Cooling Fluid	25°C

Stator – Casing Interface Contact Resistance

For the previous thermal analysis completed it was assumed that a contact resistance between the motor casing and the stator was a constant value of 4000W/m²K. Since the contact resistance of interfacing metallic sheets is quite complex, this value is a fairly unreliable estimate. Taking values from literature for the upper and lower bounds of thermal resistance between machined aluminum and steel faces, a study can be completed to determine the effect that this has on temperatures within the motor [55].

Table 24 Peak Motor Temperature Sensitivity to Stator-Casing Interface Resistance

Component	4000W/m²K	40000W/m²K
Stator	94.1°C	86.94°C
Polymer	173.8°C	167.7°C
Coils	176.1°C	169.9°C

The peak temperature in important motor components is reduced from the reduction of the interface resistance between the stator and casing. However, temperature values are not drastically affected by the change, with a 1000% reduction in interface resistance resulting in only a 1.3% change in peak motor temperature.

Error in Polymer Thermal Conductivity

As mentioned in the polymer development section of this work, the process of calculating thermal conductivity of polymer materials has a ±5% error. Given that the thermal conductivity of the polymer composite was tested to be 2W/mK, the error from the measurement could put the thermal conductivity of the material between 1.9 and 2.1 W/mK.

Table 25 Peak Motor Temperature Sensitivity to Potting Compound Thermal Conductivity

Component	1.9W/mK	2W/mK	2.1W/mK
Stator	95.05°C	94.1°C	92.7°C
Polymer	178.6°C	173.8°C	169.2°C
Coils	180.9°C	176.1°C	171.45°C

Accommodating for ±5% error in the thermal conductivity measurement of the potting material resulted in a change of about ±5°C, or 5.3% change, in peak motor temperature. This change in motor temperature is very significant considering the amount of change in the thermal conductivity of the polymer composite.

Since the developed thermal model is very sensitive to the thermal conductivity of the polymer composite, further investigation into the effect of thermal conductivity was completed. To determine the effect of potting compound thermal conductivity on motor temperature, a more wide range of thermal conductivities was simulated.

Figure 44 displays how the peak motor temperature changes as the thermal conductivity of the polymer-potting compound is changed from 1 to 10W/mK. At low potting compound thermal conductivities, the sensitivity of peak motor temperature to an incremental change is very significant. As the thermal

conductivity of the polymer composite increases, the effect is has on the peak motor temperature decreases. From thermal conductivities of 1 to 3, the percent change in peak motor temperature ranges from about 33% to 20% per w/mK of thermal conductivity. That is, a small change in potting compound thermal conductivity results is a large change in peak motor temperature. At thermal conductivities above 3 W/mK the percent change in peak motor temperature drops to about 10% or below. For this reason, if further development of a thermally conductive potting compound is to be completed, a thermal conductivity value at 4 W/mK is the best target to aim for. Any thermal conductivity values higher than 4 W/mK, a considerable amount of diminishing returns occurs.

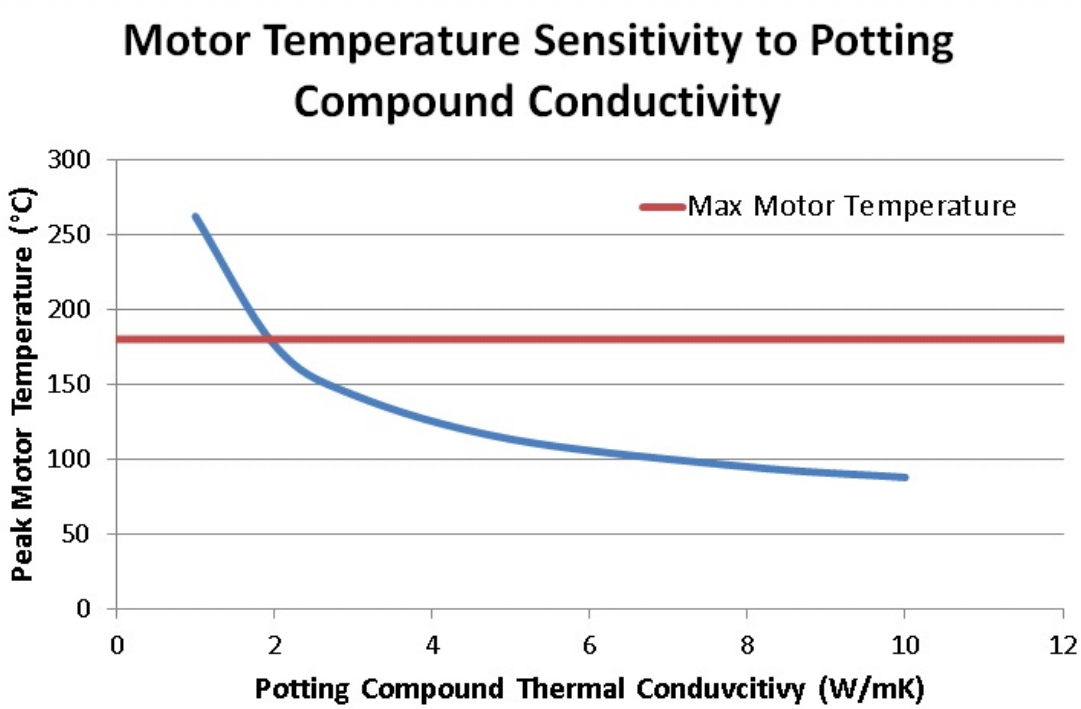

Figure 44 Peak Motor Temperature Sensitivity to Potting Compound Thermal Conductivity

Channel Thermal Conductivity

For the previous simulations, it was assumed that he cooling channel was made out of a specialized thermal plastic material that has thermal conductivity of 20W/mK. It will be investigated how the reduction in thermal conductivity of the cooling channel will affect the overall peak motor temperature. Two additional materials will be considered for the cooling channel, a material that has the same thermal conductivity as the potting material and polycarbonate. Polycarbonate is assumed to have a thermal conductivity of 0.2W/mK.

Table 26 Peak Motor Temperature Sensitivity to Cooling Channel Thermal Conductivity

Component	0.2W/mK	2W/mK	5W/mK	20W/mK
Stator	155.45°C	114.9°C	104.7	94°C
Polymer	255.45°C	191°C	181.9	173.8°C
Coils	260.8°C	193.3°C	184.3	176°C

Similar to what occurs when the conductivity of the potting compound is increased, the effect cooling channel conductivity decreases as its thermal conductivity increases. However, if the thermal conductivity of the axial channel is as low as that of a typical polymer, 0.2W/mK, the peak motor temperature increases significantly.

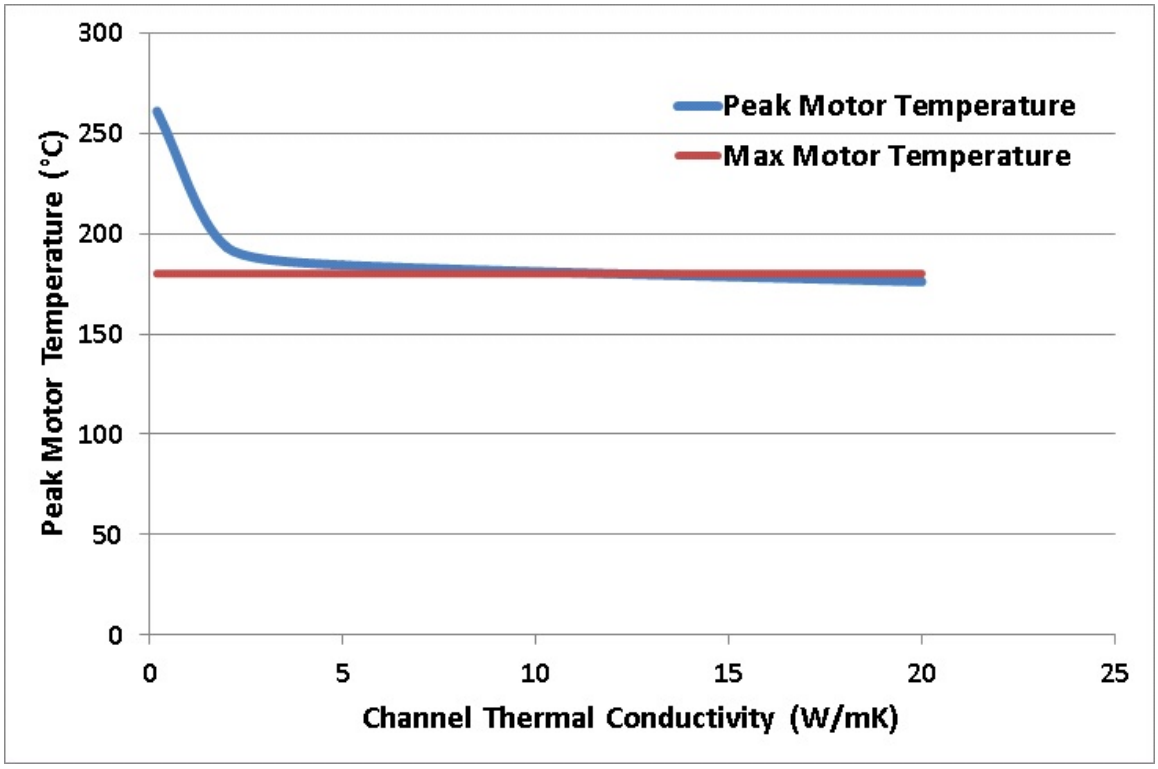

Figure 45 Peak Motor Temperature Sensitivity to Axial Channel Thermal Conductivity

Again, similar to that of the sensitivity analysis for the polymer-potting compound, after about 4W/mK a diminishing returns is experienced. Therefore, materials that have a thermal conductivity of at least 4 W/mK should be used as cooling channel material.

Cooling Fluid Temperature

In order to directly compare the effect of the cooling fluid temperature on the overall peak motor temperature, several simulations were completed at different cooling fluid temperatures. From literature, the maximum temperature of a cooling fluid operates at is roughly 75°C [59]. A midpoint simulation with a cooling fluid temperature of 50°C was also completed.

Table 27 Peak Motor Temperature Sensitivity to Cooling Fluid Temperature

Component	25°C Cooling Fluid	50°C Cooling Fluid	75°C Cooling Fluid
Stator	94°C	115.9°C	135.8°C
Polymer	173.8°C	194.9°C	214.6°C
Coils	176°C	197.2°C	216.9°C

It is clear that to see from Table 27 that the temperature of the cooling fluid has a significant impact on the peak motor temperature. It is difficult to say at which temperature the cooling fluid would be since that depends on a number of factors such as load cycle of the motor, heat exchanger size and efficiency and ambient temperature used to cool the cooling fluid. These factors are considered out of the scope of this work. For this study, only the effect of the cooling fluid temperature on the peak motor temperature is investigated, not the operating points in which the motor is being used.

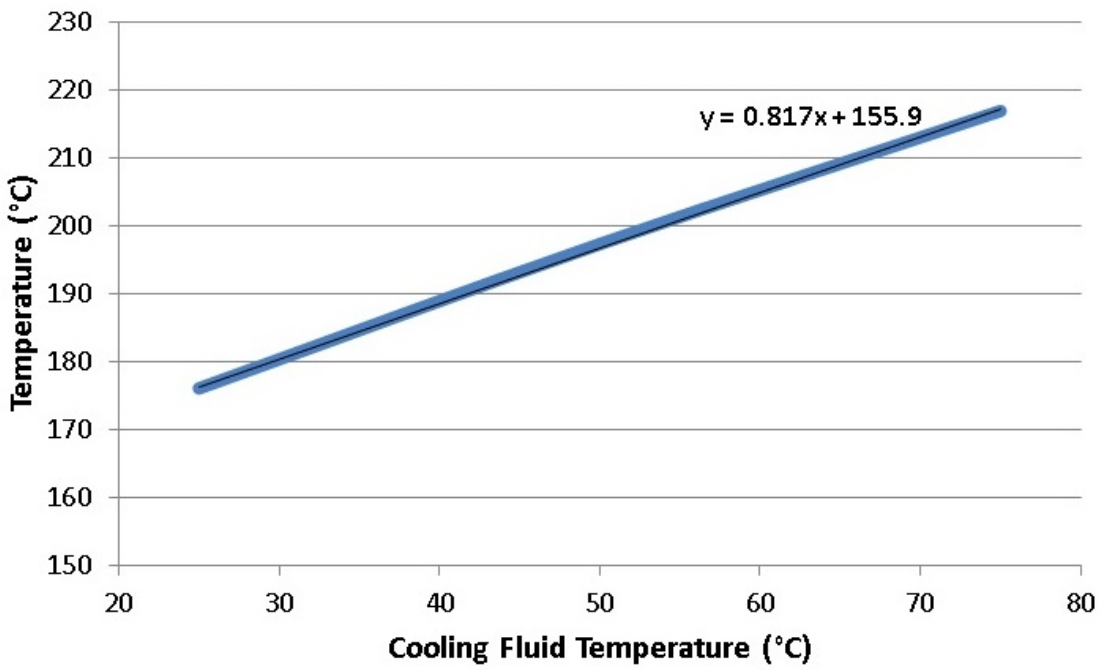

Figure 46Peak Motor Temperature Sensitivity to Coolant Temperature

Through the simulation results available, that the motor's peak temperature will increase almost linearly with the cooling fluid temperature. The equation of the line describes the relationship between coolant temperature and peak motor temperature. For every increase of 1°C of coolant temperature, the peak motor temperature goes up 0.82°C.

7. Conclusions

The development of thermally conductive polymer composites has many advantages in the role of motor cooling. By producing a polymer-potting compound that has a high thermal conductivity, the amount of heat generated within a motor stator can be significantly reduced. A thermally conductive polymer composite was developed that had a 250% increase in thermal conductivity when compared to the base matrix materials. However, given that the polymer must be vacuum infusible to be implemented into the motor stator, the maximum developed thermal conductivity of a polymer composite is significantly lower. While maintaining the ability to e vacuum infused, the best performing polymer composite achieved a thermal conductivity of 1.25 W/mK, a 50% increase over the base matrix polymer.

Given the data that was presented in the study, it can be concluded that the implementation of axial cooling channels into a motor has a considerable effect on the temperature of critical components in the motor when operating at both continuous and transient operation. When comparing the effect of axial cooling to a motor that was not axial cooled, peak motor temperatures reduced by up to 35°C when operating at stead state. This temperature reduction is assuming a polymer-potting compound that is capable of achieving a thermal conductivity of 2 W/mK while still remaining implementable into the motor stator through vacuum infusion. Furthermore, peak motor output power was increased by 60kW, or 66%, once axial cooling was implemented, again assuming a potting compound that is capable of achieving 2W/mK of thermal conductivity.

Finally, it was determined that the peak temperature of the motor is incredibly sensitive to the thermal conductivity of the polymer potting compound as well as the axial cooling channel. At small values of thermal conductivity, the peak motor temperature is very sensitive to incremental changes in thermal conductivity. Moreover, as the thermal conductivity of the polymer potting compound and axial channel increase, the sensitivity of the motor temperature greatly reduces. It was determined that an ideal thermal conductivity for both the axial cooling channel and the polymer potting compound was 4 W/mK. Beyond this value, diminishing returns results in a small sensitivity of motor temperature to thermal conductivity.

References

[1] B. Bilgin, P. Magne, P. Malysz, Y. Yang, V. Pantelic, M. Preindl, A. Korobkine, W. Jiang, M. Lawford and A. Emadi, "making the Case for Electrified Transportation," *IEEE Trans. on Transportation Electrification,* vol. 1, no. 1, pp. 4-17, 25 May 2015.

[2] M. A. Kromer and J. B. Heywood, "Electris Powertrains: Opportunitirs and Challenges in the U.S. Light-Duty Vehilce Fleet," Laboratory for Energy and the Environment, Cambridge, 2007.

[3] M. Krishnamurthy, C. S. Edrington, A. Emadi, P. Asadi, M. Ehsani and B. Fahimi, "Making the Case for Applications of Switched Reluctance Motor Technology in Automotive Products," *IEEE Trans. On Power Electronics,* vol. 21, no. 3, pp. 659-675, May 2006.

[4] B. Bilgin and A. Emadi, "Electric Motors in Electrified Transportation," *IEEE Power Electronics Magazine,* vol. 1, no. 2, pp. 10-17, June 2014.

[5] M. K. Yoon, C. S. Jeon and S. K. Kauh, "Efficincy Increase of an Induction Motor byImproving Cooling Performance," *IEEE Trans. on Energy Conversion,* vol. 17, no. 1, pp. 1- 6, March 2002.

[6] ASM International, "Properties and Selection: Nonferrous Alloys and Special-Purpose Materials," *ASM Metals Handbook,* vol. 10, no. 2, p. 941, 1990.

[7] W. H. Yeadon and A. W. Yeadon, Handbook of Small Electric Motors, New York: McGraw-Hill, 2001.

[8] M. Cirani, S. Eriksson and J. Thunberg, "Innovative Design for Flux Leakage Reduction in IPM Machines," *International Conference on Electrical Machines (ICEM),* pp. 2671-2676, Sept. 2012.

[9] H. Zhou, S. Zhang and M. Yang, "The effect of heat-transfer passages on the effective thermal conductivity of high filler loading composite materials," *Composites Science and Technology,* vol. 67, pp. 1035-1040, 2007.

[10] A. T. Collins, E. C. Lightowlers and P. J. Dean, "Lattice Vibration Spectra of Aluminum Nitride," *Physical Review,* vol. 158, no. 3, pp. 833-838, June 1967.

[11] O. Madelung, U. Rossler and M. Schulz, "Semiconductors: Group IV Elements, IV-IV and II-IV Compounds. Part A- Lattice Properties," in *Landolt-Börnstein - Group III Condensed Matter*, vol. 41, Berlin, Springer Materials.

[12] CoorsTek, "ADVANCED NITRIDE MATERIALS," 2015. [Online]. Available: http://www.coorstek.com/materials/ceramics/nitrides.php. [Accessed 24 June 2015].

[13] Z. Han and A. Fina, "Thermal conductivity of carbon nanotubes and their polymer nanocomposites: A review," Harbin University of Science and

Technology, Harbin, China, 2010.

[14] Z. Lin, Y. Liu, K.-s. Moon and C.-P. Wong, "Enhanced Thermal Transport of Hexagonal Boron Nitride Filled Polymer Composite by Magnetic Field-assisted Alignment," *Electronic Components and Technology Conference (ECTC),* pp. 1692-1696, May 2013.

[15] K. C. Yung and H. Liem, "Enhanced Thermal Conductivity of Boron Nitride Epoxy-Matrix Composite Through Multi-Modal Particle Size Mixing," *Journal of Applied Polymer Science,* vol. 106, pp. 3587-3591, August 2007.

[16] I. Jo, M. T. Pettes, J. Kim, K. Watanabe, T. Taniguchi, Z. Yao and L. Shi, "Thermal Conductivity and Phonon Transport in Suspended Few-Layer Hexagonal Boron Nitride," *Nano Letters,* vol. 13, pp. 550-554, 2013.

[17] R. Krishnan, Switched Reluctance Motor Drives, Boca Raton: CRC Press, 2001.

[18] P. H. Mellor, D. Roberts and D. R. Turner, "Lumped parameter thermal model for electrical machines of TEFC design," *Electric Power Applications, IEEE Proceedings B,* vol. 138, no. 5, pp. 205-218, Sept. 1991.

[19] R. Huaytia, "Skin and Proximity Effect Analysis of Traction Motor," M.S. Thesis, Elec. Eng., Royal Inst. Tech., Stockholm, Sweden, 2012.

[20] D. A. Gonzalez and D. M. Saban, "Study of the Copper Losses in a High-Speed Permanent-Magnet Machine With Form-Wound Windings," *IEEE Trans. on Industrial Electronics,* vol. 61, no. 6, pp. 3038-3045, June 2014.

[21] NDT Resource Center, "Diamagnetic, Paramagnetic, and Ferromagnetic Materials," Iowa State University, 2014. [Online]. Available: https://www.nde-ed.org/EducationResources/CommunityCollege/MagParticle/Physics/MagneticMatls.htm. [Accessed 29 July 2015].

[22] NDT Resource Center, "Magnetic Domain," Iowa State University, 2014. [Online]. Available: https://www.nde-ed.org/EducationResources/HighSchool/Magnetism/magneticdomain.htm. [Accessed 29 July 2015].

[23] T. R. Kuphaldt, "Lessons In Electric Circuits -- Volume II," 2014. [Online]. Available: http://www.ibiblio.org/kuphaldt/electricCircuits/AC/AC_13.html. [Accessed 29 July 2015].

[24] J. C. Andreas, Energy-Efficint Electric Motors - Selection and Application, New York: Marcel Dekker, Inc, 1992.

[25] electrical4u.com, "Hysteresis Eddy Current Iron or Core Losses and Copper Loss in Transformer," electrical4u.com-Online Electrical Engineering, [Online]. Available: http://www.electrical4u.com/hysteresis-eddy-current-iron-or-core-losses-and-copper-loss-in-transformer/. [Accessed 26 July 2015].

[26] NDT Resource Center, "The Hysteresis Loop and Magnetic Properties," Iowa

State University, 2014. [Online]. Available: https://www.nde-ed.org/EducationResources/CommunityCollege/MagParticle/Physics/HysteresisLoop.htm. [Accessed 29 July 2015].

[27] G. E. Luke, "The Cooling of Electric Machines," *Annual Convention of the A.I.E.E,* pp. 1278-1287, June 1923.

[28] L. Song, Z. Li, J. Gao, Q. Zeng and F. Wang, "3D Thermal Analysis of Water Cooling Induction Motor used for HEV," *International Conference on Electric Machines and Systems,* pp. 534-537, 2008.

[29] S. E. S. Khwaja M. Rahman, "Deisgn of High-Efficiency and High-Torque-Density Switched Reluctance Motor for Vehicle Propulsion," *Industrial Applications,* vol. 38, no. 6, p. 8, 2002.

[30] J. Lindström, Development of an Experimental Permanent-Magnet Motor Drive, M.S. Thesis, Dept. of Power Eng. Chamlers Univ. of Tech., Göteborg, Sweden, 1999.

[31] G. D. Gagnon, "Winding end turn cooling in an electric machine". USA Patent US 8198762 B2, 12 June 2012.

[32] W. L. Soong, "Thermal Analysis of ELectrical Mahines: Limits and Heat Transfer Principles," *Power Engineering Briefing Note Series,* vol. 3, pp. 19-20, 2008.

[33] B. H. Ajoy, "Liquid Cooled Electric Motor Frame". USA Patent 0859447 A1, 19 August 1998.

[34] R. A. Himmelmann, "Cooling of Permanent Magnet Electric Machine". USA Patent 8604651 B2, 10 December 2013.

[35] E. J. Ognibene and J. Kiley, "Passive, phase-change, stator winding end-turn cooled electric machine". USA Patent US 6515385 B1, 4 February 2003.

[36] W. E. Rippel and D. M. Kobayashi, "Lamination Cooing System Formation Method". USA Patent US 20120261058 A1, 18 October 2012.

[37] P. L. Andrew and F. J. Rink Jr., "Direct-Cooled Dynamoelectric Machine Stator Core with Enhanced Heat Transfer Capabilities". USA Patent 5869912, 9 Feb 1999.

[38] S. S. Khwaja Rahman, "Concentrated winding electric motor having optimized winding cooling and slot fill". USA Patent US20040100154A1, 26 Nov 2002.

[39] K. S. J. P. A. W. D. G. J. W. B. Evangelos Trifon Laskaris, "High power density cooling of electrical machines using ceramic tubes of high thermal conductivity". USA Patent US20080143199 A1, 14 Dec 2006.

[40] E. H. Weber, "Development and Modeling of Thermally Conductive Polyer/Carbon Composites," Ph.D. Dissertation, Chem. Eng., Michigan Tech. Univ., Houghten, MI, 2001.

[41] H. Zhou, S. Zhang and M. Yang, "The effect of heat-transfer passages on the effective thermal conductivity of high filler loading composite materials,"

Composites Science and Technology, vol. 67, pp. 1035-1040, 2007.

[42] C. P. Wong and R. Bollampally, "Thermal Conductivity, Elastic Modulus, and Coefficient of Thermal Expansion of Polymer Composites Filled with Ceramic Particles for Electronic Packaging," Atlanta, 1999.

[43] Y. Agari and T. Uno, "Thermal Conductivity of Polymer Filled with Carbon Materials: Effect of Conductive Particle Chains on Thermal Conductivity," *Journal of Applied Polymer Science,,* vol. 30, pp. 2225-2235, 1985.

[44] K. Wattanakul,, H. Manuspiya and N. Yanumet, "Thermal conductivity and mechanical properties of BN-filled epoxy composite: effects of filler content, mixing conditions and BN agglomerate size," *Journal of Composite Materials,* pp. 1-14, 2011.

[45] G.-W. Lee, M. Park, J. Kim, J. I. Lee and H. G. Yoon, "Enhanced thermal conductivity of polymer composites," *Composites Part A: Applied Science and Manufacturing,* pp. 727-734, 2005.

[46] D. M. Bigg, "Thermally Conductive Polymer Compositions," *Polymer Composites,* vol. 7, no. 3, pp. 125-140, 1986.

[47] H. Ishida and S. Rimdusit, "Very high thermal Conductivty obtained by boron nitride-filled polybenzoxazine," *Thermochimica Acta,* vol. 320, pp. 177-186, 1998.

[48] X. Lu, G. Xu, P. G. Hofstra and R. C. Bajcar, "Moisture–Absorption, Dielectric Relaxation, and Thermal Conductivity Studies of Polymer Composites," *Journal of Polymer Science: Part B: Polymer Physics,* vol. 36, pp. 2259-2265, 1997.

[49] NETZSCH, "Principle of the LFA Method," NETZSCH, 2015. [Online]. Available: https://www.netzsch-thermal-analysis.com/en/landing-pages/principle-of-the-lfa-method/. [Accessed 27 July 2015].

[50] ASTM Standard E1461 - 13, 2013, "Standard Test Method for Thermal Diffusivity by the Flash Method," in *ASTM International*, West Conshohocken, PA, 2013, DOI: 10.1520/E1461-13.

[51] ASTM Standard E2585 - 09, 2009, "Standard Practice for Thermal Diffusivity by the Flash Method," in *ASTM International*, West Conshohocken, PA, 2009 DOI: 10.1520/E2585-09.

[52] NETZSCH, "Laser Flash Apparatus LFA 457 MicroFlash - Method, Technique, Applications of Thermal Diffusivity and Thermal Conductivity," [Online]. Available: https://www.netzsch-thermal-analysis.com/en/products-solutions/thermal-diffusivity-conductivity/lfa-457-microflash/. [Accessed 27 July 2015].

[53] ASTM Standard E1269 - 11, 2011, "Standard Test Method for Determining Specific Heat Capacity by Differential Scanning Calorimetry," in *ASTM International*, West Conshohocken, PA, 2011, DOI: 10.1520/E1268-11.

[54] "Ansys CFX," [Online]. Available: http://www.ansys.com/Products/Simulation+Technology/Fluid+Dynamics/Fluid+Dynamics+Products/ANSYS+CFX. [Accessed 2 July 2015].

[55] D. Stanton, A. Boglietti and A. Cavagnino, "Solving the More Difficult Aspects of Electric Motor Thermal Analysis in Small and Medium Size Industrial Induction Motors," *IEEE Trans. on Energy Conversion,* vol. 20, no. 3, pp. 620-628, September 2005.

[56] Dassault Systems, "Solidworks Help," [Online]. Available: http://help.solidworks.com/2012/English/SolidWorks/cworks/Thermal_Contact_Resistance.htm. [Accessed 22 July 2015].

[57] L. Siesing, A. Reinap and M. Andersson, "Thermal properties on high fill factor electrical windings: Infiltrated vs non infiltrated," in *Electrical Machines (ICEM), 2014 International Conference on*, Berlin, Germany, Sept. 2014.

[58] T. Smy, D. Walkey and S. K. Dew, "A 3-D Thermal Simulation Tool for Integrated Devices - Ator," *IEEE Trans. on Computer-Aided Design of Integrated Circuits and Systems,* vol. 20, no. 1, pp. 105-115, 2001.

[59] E. L. Filip, "Evaluation and Application of Thermal Modeling for High Power Motor Improvements," M.S. Thesis, Mech Eng, Virginia Poly.Inst. and State Univ., Blacksburg, VA, 2010.